2007:028

MASTER'S THESIS

# Targeting of High Quality Groundwater in the Province of Vientiane, Laos, PDR

Titus Adewale Olowokudejo

Luleå University of Technology

MSc Programmes in Engineering
MSc programme in Applied Geoscience and Mining
Department of Chemical Engineering and Geosciences
Division of Applied Geophysics

2007:028 - ISSN: 1653-0187 - ISRN: LTU-PB-EX--07/028--SE

# MASTER'S THESIS

# Targeting of High Quality Groundwater In The Province of Vientiane, Laos PDR

A Minor Field Study

**OLOWOKUDEJO TITUS ADEWALE**

**MASTER OF SCIENCE PROGRAMME**

Lulea University of Technology, Sweden
Department of Chemical Engineering and Geosciences
Division of Ore Geology and Applied Geophysics

## Supervisor

**Sten-Ake Elming**
Professor of Applied Geophysics
Division of Ore Geology and Applied Geophysics
Lulea University of Technology
971 87 Lulea
Sweden

## Dedication

This project is dedicated to El-shaddai and to those who determine to succeed in life

*Until we rely on the dependable help of God sweating continues. For the destiny of a man is not in the hand of another man.……..Titus*

## Acknowledgement

This work could never have been completed without help and support from both people in Sweden and Laos, PDR. These persons, who assisted me in a friendly and humoristic manner, made it a pleasure to perform this thesis. I received help from many, but the persons below deserve extra credit.

First of all I would like to express my profound gratitude to my supervisor Professor Sten-Ake Elming, who magnificently supported me with invaluable advice throughout the whole work and help me with both practical and theoretical problems.

I would also like to take the opportunity to thank Dr Khamphouth Phommasone, National University of Laos for inviting us to Vientiane, helping us during the fieldwork and providing us with necessary information.

My deepest appreciation goes to Swedish Internal Development Cooperation Agency (SIDA) for providing the main financial funding.

I highly appreciate the role and contributions of Nils Perttu, PhD student of my supervisor.

Special mention is hereby made of Professor Lennart Widenfalk for his fatherly advice. My appreciation goes to my beloved wife Mrs. Oluwatoyin Morenike Olowokudejo for her motherly role and financial support. Finally, I thank my friends that we studied together in Lulea University for their unalloyed support, people like Sanusi Olarenwaju, Amida Kamorudeen, Ikumapayi Fatai and Awe Samuel.

# Contents

## List of Figures

## List of Table

## Abstract

Magnetic Resonance Soundings (MRS) has been proven to be an efficient tool for detecting groundwater in the northern part of Vientiane, Laos PDR. This is the first time of testing in Laos's area where the magnitude of earth magnetic field is higher than 43,700 nT. Testing of MRS here would have the advantages of high penetration depth and amplitude of MRS signals produced by the hydrogen proton in the subsurface water layers. Good signals have been achieved by carefully selecting sites of low background noise (< 1,000 nV), low magnetic susceptibility of subsurface and /or surface soil (< $10^{-3}$ SI), and small variation of a local earth magnetic field. The MRS results agree well with the subsurface geological structures and the water productivity provided by boreholes data in the vicinity of investigated area. The higher water productivity was found in the area of thicker soft sediment layer.

Schlumberger VES has been conducted in the same target area of groundwater exploration and their results were also served for MRS inversion. Comparison results of VES and MRS have been made and they are generally consistent. At the site where a water-bearing layer in the deeper parts is suggested by MRS with a detection of low signal amplitude and large variation of observed decay time, the VES result also confirmed that the layer is very high conductive.

This case-study demonstrates that the MRS and VES methods can be an effectively selective method for groundwater investigation and can be integrated with other geophysical methods to fulfill groundwater database in Laos PDR.

# 1.0 Introduction

The importance of groundwater for the existence of human society cannot be overemphasized. Groundwater is one of the major sources of drinking water in Lao PDR both urban and rural areas but it is not sufficient to carter for the entire country. Most of the village people depend on homemade 5 – 15m deep dug wells without lining for their domestic water use. A few depend on wells with hand-pumps. In areas with very high water tables these dug wells are prone to be contaminated. The incidence of water-borne diseases is at its highest during the dry season due to the shortage of potable water and the usage of shallow well water with poor water quality. According to the Ministry of Public Health's third five year plan (1992 - 1996), 50 % of those who died in 1991 were under the age of five and a high estimate of maternal mortality of 580 per 100 000 live births was given. One of main causes of mortality for persons under the age of five was diarrhea (dysentery and dehydration) due to water-borne diseases, and the main cause of maternal mortality was a lack of safe water.

Groundwater makes up nearly 70% of all the worlds' freshwater; only 0.2% is found in lakes, streams or rivers and 30% is bound up in snow and ice on mountains and in the Polar Regions. As rivers and lakes tend to be supported by groundwater, it is not exaggerating to say that almost all the water we use for agriculture, industry and drinking water is either groundwater or has been groundwater at some point in the hydrologic cycle as shown in figure 1-1 (Institute for Global Environmental Strategies, IGES 1987).

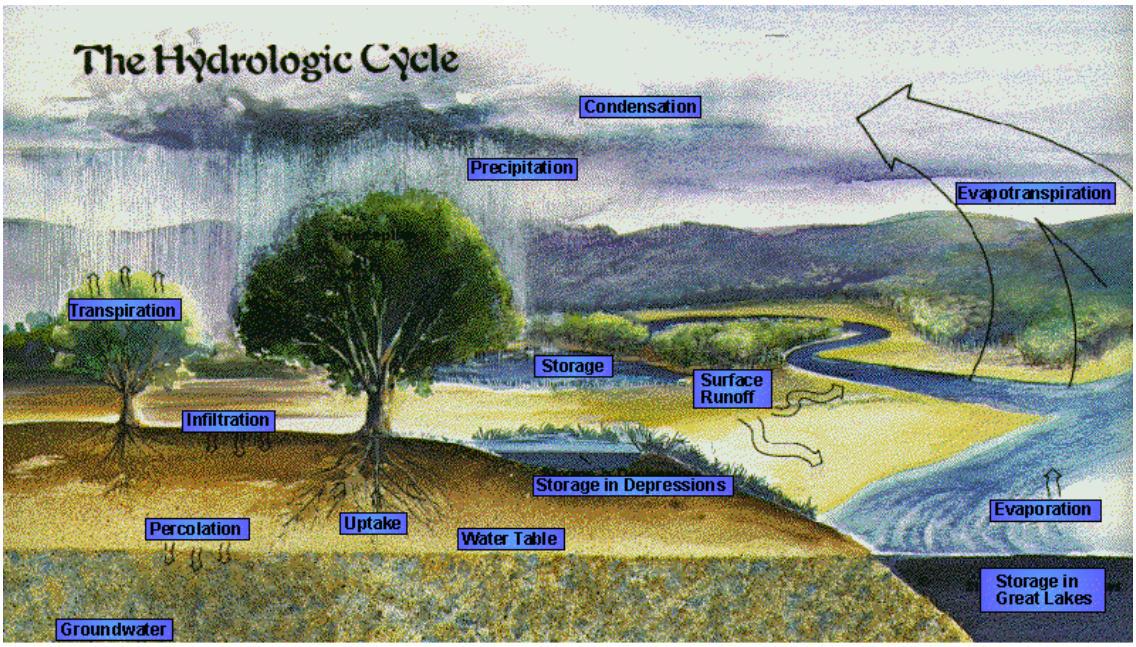


Figure 1-1 Hydrological cycle

The demand for water has increased over the years and this has led to water scarcity in many parts of Lao PDR. The situation is aggravated by the problem of water pollution or contamination. Laos is heading towards a freshwater crisis mainly due to improper management of water resources and environmental degradation, which has led to a lack of access to safe water supply to thousands of people. This freshwater crisis is already evident in many parts of Laos, varying in scale and intensity depending mainly on the time of the year (Ministry of Agriculture and forestry, Laos PDR 1998). Groundwater crisis is not only as a result of natural factors; but also caused by human actions. During the past two decades, the water level in several parts of the country has been falling rapidly due to an increase in extraction. The number of wells drilled for irrigation of both food and cash crops have indiscriminately increases. Laos PDR steadily rising population and changing lifestyles has also increased the domestic need for water. The water requirement for the industry also shows an overall increase. Intense competition among users- agriculture, industry, and domestic sectors – is driving the groundwater table lower. The quality of water is getting severely affected because of the widespread pollution of surface water (Ministry of Agriculture and forestry, Laos PDR 1998).

### *1.1 Hydro-geology*

The only hydro-geologic information currently available for the Lao PDR overall is the Preliminary Appraisal of the Hydrogeology of the lower Mekong Basin Published by the interim Mekong committee in 1986. It shows that the Lao PDR is divided into two geological areas, the Annamian strata occupying the most northern and eastern regions and the Indosinian sediments, mainly along the Mekong River. The Annamian region includes granites, metamorphic and palaeozoic rocks. The Indosinian region consists of sandstones, siltstones, shale, mudstones, limestone, conglomerates and basalt.

There are three different aquifer systems; the Annamian, Indosinian and Limestone. The Annamian aquifers occur at random. They are local systems that discharge locally into the river or its tributaries. As local flow systems, they are not part of regional flow systems and will not carry pollution into the regional groundwater system. Potential water supply from groundwater in northern Lao is considerable in view of the high amount of recharge available. Water quality should be reasonably good and for the most part potable but water will be iron rich. Yields up to 5 litres/sec can generally be anticipated.

The Indosinian group of aquifers, which have regional flow, includes rock strata of the Indosinian Moyennes and Superieures and is relatively young. They are mostly freshwater sediments, although three are horizons of brackish water, and one major zone of saline water yields of 12 to 24 litres/sec can be developed. Alluvial aquifers associated with Mekong River sedimentary deposits are not rated highly as aquifers.

Limestones in the central region are strictly Annamian in age, but their location places them logically in the Indosinian flow system. They have been described as having enormous groundwater resources.

No notable investigation and study on the groundwater appears to have been conducted in the Lao PDR. In the early 1990s, the Mekong Secretariat conducted a project ‘Review of Groundwater Data in the Lower Mekong Basin’ and installed 18 observation wells: ten were installed in the Vientiane plain and the rest along the Mekong River. The observation revealed the interesting fact that the Mekong River has very little influence on aquifers in the Vientiane plain. Groundwater will be further developed as the main source of urban and rural water supply and small - scale irrigation in lowland areas far from surface water resources, such as southern and

western Champassak province and the hinterlands of the Sebang Fai, Sebang Hieng and Sedone river valleys (Ministry of Agriculture and Forestry, Laos PDR 1998).

### *1.2 Objectives of the Project*

This thesis is part of the first phase of a large project in Laos PDR. Its purpose is to contribute to developing methods for estimation of the quality of groundwater using non-destructive geophysical techniques such as Electrical resistivity and magnetic resonance sounding (MRS) methods.

The main objectives are;

1) targeting of high quality groundwater in the province of Vientiane.
2) correlating the subsurface lithologies in the study area with borehole data
3) delineating the vertical variation of subsurface resistivity by using electrical method coupled with magnetic resonance soundings.
4) determing the depth of various aquiferous zones.
5) evaluating the quality of the groundwater on basis of electrical conductivity.
6) evaluating the overall usefulness, reliability and applicability of the MRS soundings in the province of Vientiane and eventually the applicability of the technique in the other areas with similar geology.

### *1.3 Expected contribution to knowledge*

- This project is expected to reveal aquifer, their relations to subsurface lithologic setting and natural salt contamination.
- The work is expected to serve as a reference for future workers that may be interested in the groundwater quality in the province of Vientiane, Lao PDR.

### *1.4 Research methodology*

In order to achieve the study objectives, a three-stage programme was adopted; the inception stage (pre-field work), field work and post field work stage (data analysis and final reporting). The study was projected to complete within a period of four years. The inception study was carried in April 2006. The first field work took place between January 5$^{th}$ and February 1$^{st}$ 2007. Data analysis and reporting were completed in April 2007.

### *1.5 Previous work*

Japan International Cooperation Agency has carried out a geophysical survey in part of Lao PDR including sixteen Vertical Electrical Soundings to investigate the geological structure and resistivity variation of the lithologies for sitting boreholes. Also aerial photo interpretation was done in the area to understand the main stratigraphic and tectonic features and water levels were measured in the local wells.

The old wells constructed by United State Agency for International Development (USAID) and United Nation Development Programme (UNIFES) in the past have no documentation. Thus, the existing well structures are almost indefinite. According to measurements in a number of deep wells, the well depths are shallower than the original drilling depths. This is because the wells were originally drilled in an impervious layer of mudstone and shale lying under the aquifer. As the drilling was done without a casing, the bore portion was buried by an inflow of sand and silt from the aquifer distributed in the upper portion of the borehole (Japan International Cooperation Agency, 1992).

### *1.6 Study Area*

The study areas are located at Phathao (18.32899 N, 102.65272 E) and Ban Pak Hang (18.28525 N, 102.6732 E), in the Vientiane province some 40km north of Vientiane city, the capital of Lao PDR (Fig.1-2). The area is an agricultural district where many villages are ranging and the villagers are mainly using dug wells as their main water sources. However, most of the dug wells usually go dry during the dry season and the water is also polluted due to the infiltration of domestic waste or excreta of live-stock. The project area has many small undulating hills, sand and clay, shale, gravel, shingle, sand, kaolinite and lignite, which are the dominating type of sediments. (Figure 1-3)

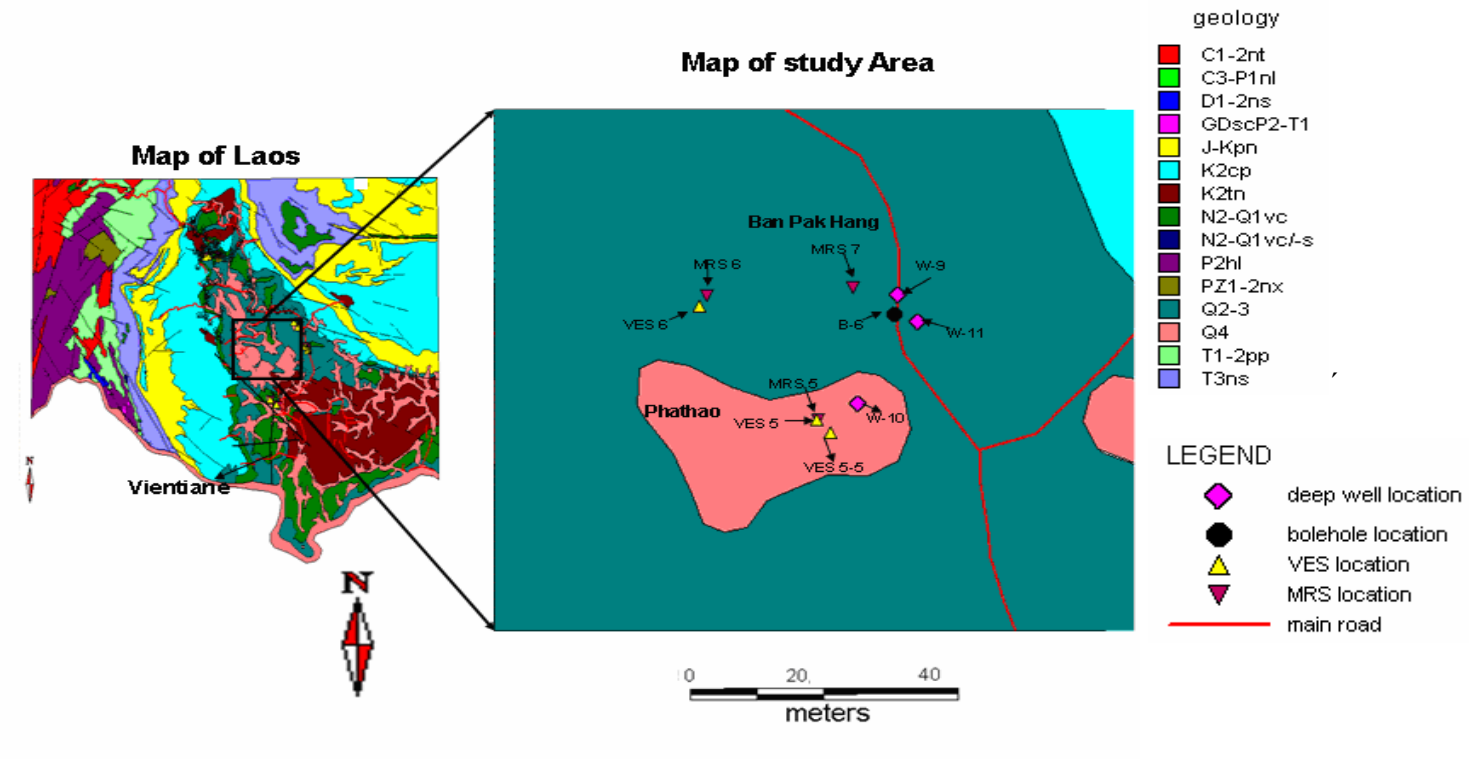


Figure 1-2. Base Map and its legend

### *1.7 Interpretation of Geology of the Laos*

| **Denotation** | **Interpretation** |
|---|---|
| **$Q_4$** | Sand, gravel, shingle clay and lignite |
| **$Q_{2-3}$** | Sand and clay, shale, gravel, shingle, sandy, kaolinite and lignite |
| **$N_2Q_{1VC}$** | Vientiane formation: Gravel, shingle, sandy kaolinite and laterite |
| **$K_2tn$** | Tha Ngon formation: Na-salt, claystone, siltstone, calcareous claystone bearing siltstone, potash salt, gypsum and anhydrite, rhyolite and tuff |
| **$K_2cp$** | Champa formation: sandstone, siltstone, brownish sandstone, white arkose sandstone, quartz-feldspar |

| | |
|---|---|
| **J-Kpn** | Phu Pha Nang formation: sandstone bearing mica white siltstone and brown sandstone, quartzite sandstone |
| **$T_3$ns** | Nam set formation: Black sandstone, siltstone and claystone bearing white mica angular purplish clay, limestone and conglomerate |
| **$T_{1-2}$pp** | Phu Lek Pha formation: Conglomerate sandstone composition reversal layer claystone and shale, calcareous sandstone, grey limestone, rhyodacite, white felsite, rhyolite and tuff |
| **$P_2$hl** | Houei La formation: sandstone, brown claystone, grey siliceous shale agglomerate, basalt, green andesite basalt and tuff. |
| **$C_3P_1$nl** | Na Lang formation: Grey laminated to massive limestone, black dolomite limestone |
| **$C_{1-2}$nt** | Nam Thom formation: Green sandstone, claystone, gravel shingle, lentigular limestone black siltstone, coal shale |
| **$D_{1-2}$ns** | Na Sa formation: Weathered limestone black siliceous limestone, green claystone, shale, calcareous siltstone and calcareous shale |
| **$PZ_{1-2}$nx** | Nam Xai formation: Shale, serisitic shale, quartzite, green dolorite, shale |

The local geology of the study area is $Q_4$, $Q_{2-3}$, $N_2Q_1$vs and $K_2$tn

(a) Testing of noise levels


(b) Collection of MRS data

Figure 1-3 Pictures taken during site investigation

# 2.0 Area Description

## *2.1 Laos*

The Lao People's Democratic Republic is a socialist republic in Southeast Asia, bordered by Myanmar (Burma) and the People's Republic of China to the northwest, Vietnam to the east, Cambodia to the south, and Thailand to the west (Fig:1-4). Laos traces its history to the kingdom of Lan Xang or Land of a million Elephant, which existed from the fourteenth to the eighteenth century. After a period as a French colony, it gained independence in 1949. A long civil war ended when the communist Pathet Lao came to power in 1975. Private enterprise has increased since the mid-1980s, but development has been hampered by poor communications in the heavily forested and mountainous landscape. The country's total area is 236 800km$^2$. About 20 percent of the land is flatland (70 -200 msl); the other 80 percent is sloping hillsides and mountains (200 - 2 820 msl). The Lao PDR has a tropical monsoon climate: annual rainfall averages 1 000 – 1 500 mm in most of the country. While there is an abundance of forest and water resources with potential for development, both floods and drought are commonly experienced. The population is about 5 million persons with some 48 ethnic groups.

Despite this, the economy of Laos grew at 7.2% in 2006 (world fact book, 2006), 35$^{th}$ fastest in the world. Eighty percent of the employed practice subsistence agriculture. The country's ethnic make-up is extremely diverse with only around 60% belonging to the largest ethnic group, the Lao (Kramer, 1999).


Fig.2.1 Map of Laos People's Democratic Republic

### *2.2 Culture of Laos*

Theravada Buddhism is a dominant influence in Lao culture. It is reflected throughout the country from language to the temple and in art, literature, performing arts, etc. However many elements of Lao culture predate Buddhism. For example, Laotian music is dominated by its national instrument, the khaen, a type of bamboo pipe that has prehistoric origins. The khaen traditionally accompanied the singer in lam, the dominant style of folk music. Among the various lam styles, the lam saravane is probably the most popular. The country has two World Heritage Sites: Luang Prabang and Wat Phou. The government is seeking the same status for the plain of Jars.

Rice is the staple food and has cultural and religious significance. There are many traditions and rituals associated with rice production in different environment, and among many ethic groups. For example, Khamu farmers in Luang Prabang plant the rice variety Khao Kam in small quantities near the hut in memory of dead parents, or at the edge of the rice field to indicate that parents are still alive (Kramer, 1999).

### *2.3 Geography*

Laos is a landlocked country in Southeast Asia and the thickly forested landscape consists mostly of rugged mountains, the highest of which is Phou Bia at 9,242 feet (2,817m), with some plains and plateaus. The Mekong Rivers forms a large part of the western boundary with Thailand, whereas the mountains of the Annamite chain form most of the eastern border with Vietnam. The climate is tropical and characterized by

monsoons. There is a distinct rainy season from May to November, followed by a dry season from December to April. The capital and largest city of Laos is Vientiane and other major cities include Luang, Prabang, Savannakhet and Pakse. In 1993, the government set aside 21% of the nation's land area as National Biodiversity Conservation Area (NBCA), which may be developed into a national park system. If completed, it is expected to be the most comprehensive and one of the finest national parks in systems in Southeast Asia. A number of animal species have been discovered or re-discovered in Laos in recent years. These include the striped or Annamite rabbit, the saola, and most recently the Laotian rock rat or kha-nyou.

Laos is divided into sixteen provinces (Kang), one municipality and special zone:

1. Attapu 2. Bokeo 3. Bolikhamxai 4. Champasak. 5. Houaphan 6. Khammouan 7. Loung Namtha 8. Louangphabang 9. Oudomxai 10. Phongsali 11. Salavan 12. Savannakhet 13. Vientiane (municipality) 14. Vientiane 15. Xaignabouli 16. Xaisomboun (special zone) 17. Xekong 18. Xiangkhoang.

The country is further divided into districts (muang).

### *2.4 Geology*

A long recognized problem in evaporite deposition is the origin and development of saline giants found in the rock record (Sloss, 1969; Hsu¨, 1972; Schreiber, 1988; Busson and Schreiber, 1997). The Maha Sarakham Formation (Cretaceous through Tertiary) on the Khorat Plateau of northeastern Thailand and Laos is a saline giant that includes one of the largest salt deposits in the world. The formation is composed of three depositional successions present in the northern Sakon Nakhon and the southern Khorat basins (Fig.2-1). Lithologies of the formation are dominated by halite with potassic minerals of sylvite (KCl) and carnallite (KCl $MgCl_2.6H_2O$), red beds and minor anhydrite, tachyhydrite ($CaCl_2.MgCl_2.12H_2O$) and borates [hilgardite, $Ca_2BCl\,(OH)_2$ and boracite, $Mg_3ClB_7O_{13}$].

Salt beds of the Maha Sarakham Formation were first discovered in groundwater wells in the Khorat Plateau (La Moreaux et al., 1959), and a preliminary investigation (Gardner et al., 1967) was carried out. Later, sylvite was found near Vientiane, and shortly thereafter, carnallite as well as sylvite was found on the Thai side. Earlier works by Hite (1971, 1974) and Hite and Japakasetr (1979) have outlined the general stratigraphy of the salt sequence and a broad overview of the depositional elements of

the Maha Sarakham Formation. Hite and Japakasetr (1979) reported a sharp boundary between the lower part of the evaporite section and the underlying Khok Kruat Formation, suggesting a possible disconformity. They also present details of the bromine chemistry of the salt deposits and propose a stratigraphic, environmental and structural evolution of the salt beds. Utha-Aroon (1993) suggested nonmarine depositional environment of the red-coloured clastics interbedded with the rock salt deposits based on their sedimentary features.

Most giant evaporite deposits are associated with marine shelf-carbonate sequences. The evaporites of the Maha Sarakham Formation, however, lie atop a thick non-marine sequence of the Mesozoic Khorat Group, are interbedded with non-marine red beds. They lack the more usual carbonates, and are found in an inland basin on continental crust. All of these features suggest a non-marine origin for the Maha Sarakham salts.

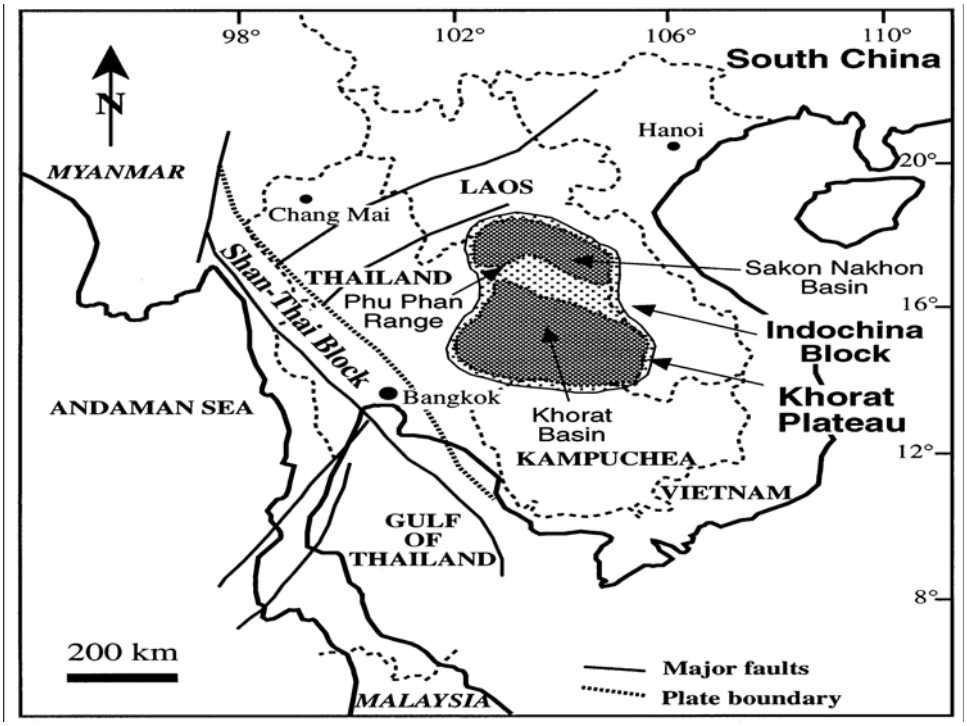


Fig.2-2. Geological map of Southeast Asia showing the general tectonic elements of the region and the location of the Khorat and the Sakon Nakhon basins.

The Khorat Plateau presently has a high escarpment of about 900 m above sea level along its western and southern edges whereas elevations of its central area are only 100–300 m above sea level. Much of the sedimentary succession that makes up the Khorat Plateau is a part of an extensive, largely non-marine depositional system in the mainland of Southeast Asia. It covers an area of 170,000 $km^2$ of the Esarn region in northeastern Thailand and central Laos, and lies between latitudes 14º and 19ºN and between longitudes 101º and 106ºE (Fig. 2-1**).** The plateau is located on the Indochina microplate and includes the Sakon Nakhon Basin to the north and the Khorat Basin to the south. These two basins are separated by the Phu Phan anticline in northeastern Thailand. The plateau is a broad synclinorium bounded in the west by the Shan Thai microplate and in the north by the South China plate. The Indochina microplate contains sediments ranging in age from Late Cambrian to Recent (Sattayarak et al., 1991; Mouret, 1994). Early to Middle Triassic collision between the Shan-Thai and the Indochina microplates along the Nan-Uttaradit suture (Sengor, 1979, 1984; Bunopas and Vella, 1992; Drumm et al., 1993), was followed by Late Triassic tectonic relaxation or extension which created half-graben basins, where thicknesses of up to 5 km of the non-marine red beds of the Khorat Group were deposited (Figure 2-2). Fluvial and lacustrine facies filled these basins with conglomerates, sandstones, and mudstones that range in age from latest Triassic to

late-Early Cretaceous (Racey et al., 1994; Mouret, 1994). The source of the Khorat rocks in Thailand is from erosion of the late Palaeozoic rocks exposed in the Nan-Uttaradit suture area in central north Thailand (Sengor, 1979; Hutchison, 1989) and possibly from eastern Laos and central Vietnam (Drumm et al., 1993). The Khorat deposits were intruded by granites of Campanian and Cenomanian age which resulted from thermal subsidence of the Khorat Plateau (Smith et al., 1996).

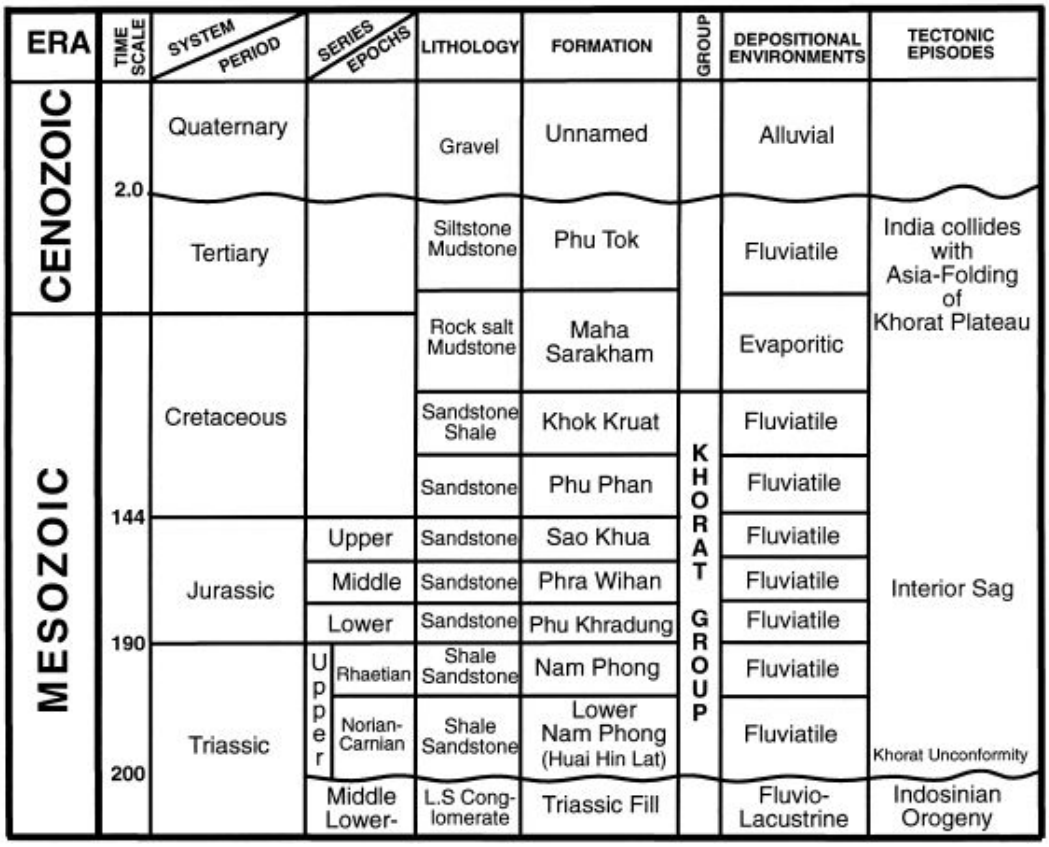


Figure 2-3 Mesozoic and the Cenozoic stratigraphy of the Khorat Basin in NE Thailand and summary of the geological history of the Indochina microplate during the Mesozoic and the Cenozoic.

During the early Paleocene, compression from the northeast due to continental collision of the Indochina microplate with southeast China plate and from backarc compression of the Shan Thai microplate to the west, resulted in uplift and erosion of about 3000 m of the Khorat sediments and the formation of the NW–SE-trending Phu Phan anticlinorium in the central part of the Khorat Plateau (Cooper et al., 1989; Mouret, 1994; Bunopas and Vella, 1992). During the Cretaceous, the Indochina microplate was located near 20ºN latitude, suggesting arid climatic conditions (Achache et al., 1983).

The Maha Sarakham Formation with its salt beds was first named by Gardner et al. (1967) and, based on palynomorphs, it is suggested to be of Albian–Cenomanian age (Sattayarak et al., 1991). The formation averages 250 m thick and is up to 1.1 km thick in the centre of the Khorat Basin. The variation in thickness appears to be due to: (1) differential subsidence before and during deposition; (2) localised tectonic

differentiation, such as development of fault-controlled highs and lows; and (3) post-depositional dissolution, particularly of the Middle and Upper Units (due to very shallow burial). Lithological, stratigraphic and mineralogical similarities of the formation in both the Sakon Nakhon and Khorat basins, suggest that a single giant evaporite basin existed at least in the area of the present-day basins (Fig.2-3).

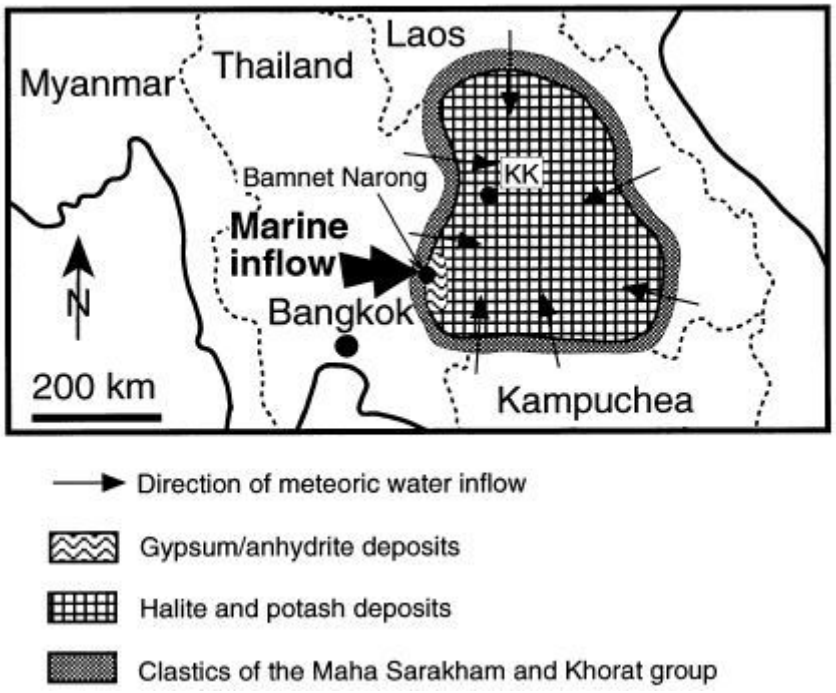


Fig.2-4. Idealised map showing the predominant rock types of the Khorat Plateau and the Maha Sarakham Formation (M.El Tabakh et al 1999). The large arrow indicates the postulated source of marine water inflow into the Khorat Plateau near Bamnet Narong area at the southwestern corner of the Khorat Plateau. KK marks the location of Khon Kaen City located in the central area of the Khorat Plateau.

### *2.5 Stratigraphy and Depositional Patterns*

The Maha Sarakham Formation comprises three distinctive depositional members (Lower, Middle and Upper) which are mainly composed of evaporites separated by red-coloured siliciclastics (Fig.2-5). All of the evaporative members contain beds composed of halite-replaced pseudomorphs of bottom-growth gypsum.

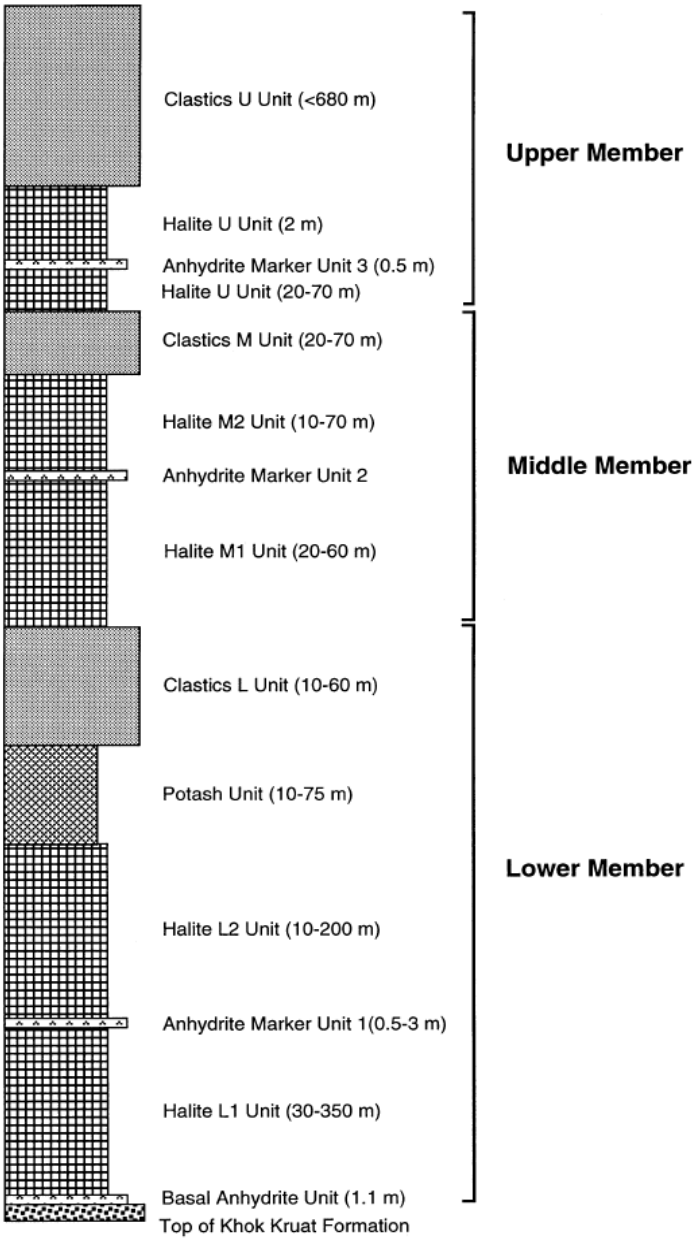


Fig. 2-5 Lithostratigraphy of a complete sedimentary section of the Maha Sarakham Formation

# 3.0 Material and Method

## *3.1 Geophysical Exploration*

There are several different geophysical methods that can be used during groundwater exploration e.g. Electrical resistivity methods, magnetic resonance soundings, seismic refraction method, electromagnetic methods, Remote sensing, TDEM, etc. For the purpose of this project, we made use of Electrical resistivity and Magnetic Resonance sounding methods.

## *3.2 Classification of Groundwater*

Subsurface waters are classified into different groups (figure 3-1) depending on its physical occurrence in the soil. Two zones can be broadly identified, which are the saturated zone where the pores are completely filled with water and the unsaturated zone where the voids contain a mixture of water, moisture and air. The unsaturated zone can be divided into three different layers. The soil moisture zone, which is essential for plants and differs in thickness depending on soil type and climate, is the top layer. The movement of water can be either upwards or downwards depending on suction or gravity. The intermediate zone is the second layer and here water is held due to intermolecular forces against the pull of gravity. The capillarity zone is the third layer and is located above the water table and the water here is held by the capillarity forces acting against gravity (Sen, 1995).

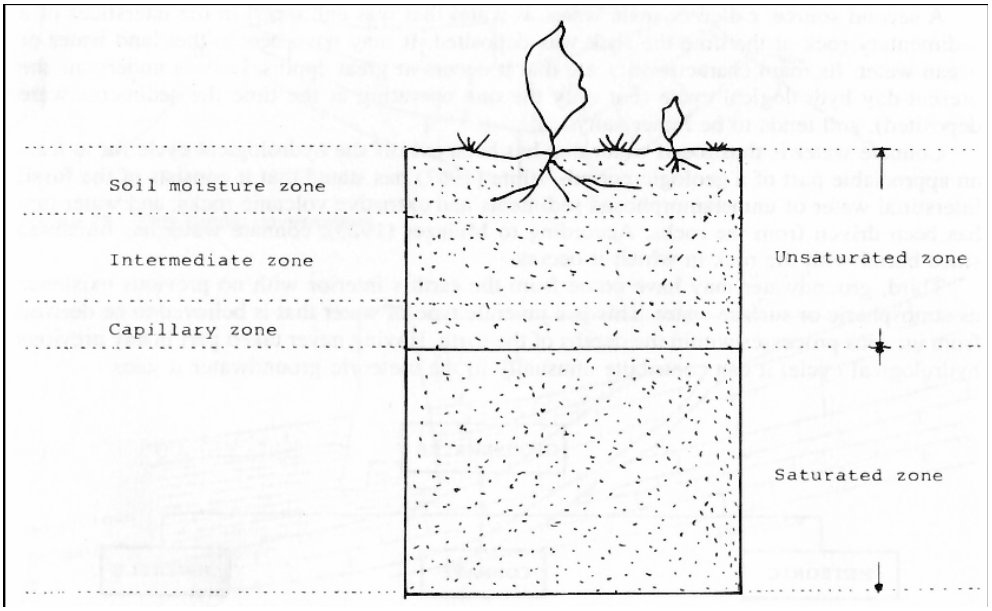


Fig: 3-1. Water zones in the lithosphere *(Sen, 1995).*

## *3.3 Water-bearing Formations*

The occurrence and movement of groundwater depends on the subsurface characteristics, like lithology, texture and structure. The different formations are classified into the following types depending on their relative permeability (Singhal and Gupta, 1999).

### *3.3.1 Aquifer*

An aquifer is a natural formation that contains sufficient amount of water and permeable

material to yield significant amount of water to wells or springs. Geological formations that serve as aquifers are gravel, sand, fractured granite etc. Aquifers can be categorized into confined-, unconfined-, perched- and leaky aquifers (Sen, 1995).

### *3.3.2 Aquiclude*

This formation is capable of absorbing water slowly, but not capable of transmitting it fast enough to yield enough water to a well. These are confining formations like crystalline rocks, clays and shale (Sen, 1995).

### *3.3.3 Aquitard*

Aquitards have insufficient permeability to act as an aquifer, but can still serve as source or interchange between neighbouring aquifers. These are usually found in silt or shale (Singhal and Gupta, 1999).

## *3.4 The Magnetic Resonance Sounding (MRS) Technique*

### *3.4.1 Historical Overview*

The magnetic Resonance Sounding (MRS) technique known also as SNMR (surface Nuclear Magnetic Resonance) or PMR (Proton Magnetic Resonance) for groundwater exploration is a relatively new application of NMR (Nuclear Magnetic Resonance). It is the only non-invasive geophysical technique with an inherent selectivity to hydrogen and therefore to groundwater (Roy and Lubczynski, 2003). The technique is site dependent; hence the geomagnetic field and electrical conductivity of the subsurface influence its performance. Legchenko et al, (2002) state that where the resistivity is larger than 50Ωm, groundwater can be detected down to 150m in areas with high intensity of the geomagnetic field and to about 100m in areas with low geomagnetic field. The first idea in the use of NMR to investigate groundwater came

from Varian in 1962 as reported in Legchenko et al (1997). The concept was then developed in the 1970s by a Russian team under Semenov who built the first MRS equipment, the Hydroscope. The technique has been used in Russia and routinely tested in many different countries and environments as reported by Schiron et al (1991), Goldman et al, (1997a), Gev et al, (1996), in Legchenko and Valla (1998). The MRS has since developed and improved. The first commercial instrument NUMIS becoming available by 1996 (Iris Instruments, 2001). Since the commercializing of the Numis Instrument, there has been a lot of interest to learn more about the method. Further tests have been done using the set of equipment in many countries; e.g. France by Legchenko et al (1995), Germany by Yaramanci et al (2002), Saudi Arabia by Legchengo et al (2002), Sweden by Elming and Wattanasen (2007) etc.

In Laos groundwater mapping has been conducted by the Japan International Cooporation Agency (JICA) that successfully used electrical resistivity method and pumping test data for detection. However, there are no reported results of MRS testing in Lao People's Democratic Republic. In Laos the magnitude of the earth magnetic field (B) is higher than 43 700 nT. Therefore a big MRS signal should be produced from groundwater as the MRS signal is proportional to $B^2$ (Roy and Lubczynski, 200b).

The latest MRS instrument version available is the NUMIS$^{Plus}$ (Iris Instruments, 2002), which is graphically presented in Fig 3-2. The instrument comprises: (1) two identical DC converters used to program a variable amount of electric energy to produce the loop excitation current in a form of required pulse moment (Q); (2) the main MRS unit used both for the AC loop excitation and signal acquisition; (3) a reel of copper cable used to lay out the loop; (4) the tuning box; (5) a high capacity rechargeable batteries used to power the system and (6) a normal PC laptop for overall system control, data recording and processing.

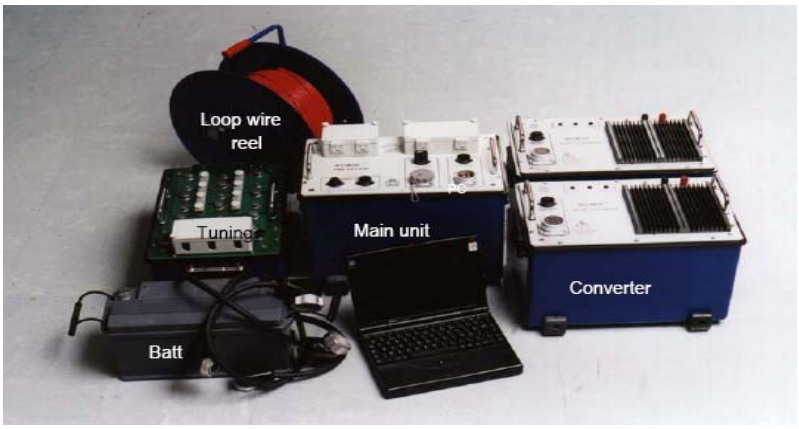


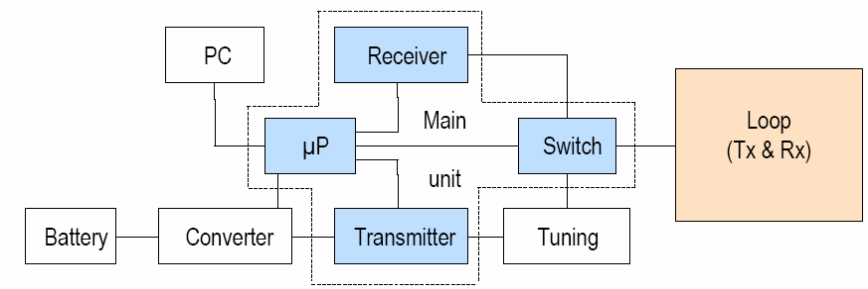


Fig.3-2: NumisPlus Magnetic Resonance System *(Iris Instruments 2002)*

### *3.4.2 MRS Principle*

The protons of the hydrogen atoms in water molecules can be described as spinning charged particles and have a magnetic moment μ. Generally, μ is aligned with the local magnetic field $B_o$ of the Earth. When another magnetic field $B_1$ is applied, the axis of the spinning protons are deflected, owing to the torque applied. Hereby, only the component of $B_1$ perpendicular to the static field, $B_\perp$, acts as the torque force. When $B_1$ is removed, the protons generate a relaxation magnetic field as they become realigned along $B_o$ while precessing around $B_o$ with the frequency

$$\omega_L = \gamma B_0 \text{, Larmor frequency} \quad f_L = \omega_L / 2\pi \text{,} \qquad (1)$$

Where γ = 0.267518 Hz /nT, the gyromagnetic ratio for hydrogen protons.

The basics of the $^1H^+$ magnetic resonance sounding are graphical presented as Figure 3-3.

The measurements are made using a loop usually with a circular or rectangular layout. The $B_1$ magnetic field is generated when an alternating current,

$$i(t) = i_0 \cos(\omega_L t), \tag{2}$$

at the Larmor frequency $f_L$ (worldwide 800 – 3000 Hz) is passed through this loop for a limited time τ, so that an excitation intensity (pulse moment) of $q = i_0\tau$ is achieved. After the current in the loop is switched off, a decaying voltage e(t) is induced in the loop by the relaxation of the protons (Legchenko and Schirov):

$$e(t) = \omega_L M_0 \int f(r) e^{-t/T(r)} \cos(\omega_L t + \vartheta(r)) B_\perp(r) \sin(0.5\gamma B_\perp(r) q) dV \tag{3}$$

Here, $M_o$ is the nuclear magnetization (the specific magnetic moment of the unit volume dV under equilibrium conditions at t = 0). $M_o$ = 3.29 x $10^{-3}$ Bo J/ (T $m^3$) for water at a temperature of 293 K. The volume fraction of water in a unit volume dV at the location r(x, y, z) is represented by f(r). T(r) is the decay time of protons at the location r(x, y, z). $B_\perp(r)$ is the component of the incident exciting field $B_1$ (normalized to 1 A) perpendicular to the static magnetic field $B_o$ of the Earth. In a conductive medium, $B_\perp(r)$ is composed of the primary field of the loop and the induced secondary field in case of high conductivity which causes the phase shift φ(r) with respect to the excitation field. Note that the argument of the sine function in Eq. (3) ($\theta = 0.5\gamma B_\perp(r)$ q) is the angle of deflection of the magnetic moment of the protons from the magnetic field of the Earth.

This signal e(t) is usually approximated by

$$e(t) = E_0 e^{-t/T} \cos(\omega_L t + \vartheta) \tag{4}$$

The envelope of this decaying voltage is directly related to the water content and to the decay time of every volume element in the underground contributing to the signal.

The initial amplitude $E_o$ at t = 0 is related only to the water content:

$$E_0 = \omega_0 M_0 \int f(r) B_\perp(r) \sin(0.5\gamma B_\perp(r) q) dV \qquad (5)$$

Using this equation, the initial amplitudes at various excitation intensities can be calculated for water-bearing (layers at different depths and with different thicknesses). Deeper water layers are reflected in $E_o$ when the q-values are higher. The amplitude of $E_o$ is thus directly related to the amount of the water and can be as large as a few millivolts.

The recorded decay time is supposed to be the relaxation time constant (spin-spin or transversal relaxation time) denoted with $T_2^*$ in the usual NMR terminology. This decay time can be of the order of a few milliseconds up to 1000 ms. It is related to the mean pore size and, therefore, grain size of the material. Clay, including sandy clay, usually has a decay time of less than 30 ms, whereas sand has one of 60 – 300 ms, gravel 300 – 600 ms, and pure water, 600 – 1000 ms (Schirov et al., 1991) as shown in table 3-1. Hydraulic conductivities can be estimated from the main grain size (Yaramanci et al., 1999).

Table 3-1: Petrophysical Information from NMR Decay Rate (After Schirov et al, 1991)

| **Signal decay rate** | **Petrophysical information** | **MRS detectability** |
|---|---|---|
| $T_2 < 3$ ms | Clay bound water | No |
| $T_2 < 30$ ms | Sandy clays | No or marginally |
| $30 < T_2 < 60$ ms | Clay sands, very fine sands | Yes |
| $60 < T_2 < 120$ ms | Fine sands | Yes |
| $120 < T_2 < 180$ ms | Medium sands | Yes |
| $180 < T_2 < 300$ ms | Coarse and gravely sands | Yes |
| $300 < T_2 < 600$ ms | Gravel deposits | Yes |
| $600 < T_2 < 1500$ ms | Surface water bodies | Yes |

The phase φ is related to the phase of the excitation signal plus with a usual phase shift of $\pi/2$ due to electromagnetic coupling. If the electrical conductivity of the ground is negligible, $B_{\perp}(r)$ will have a phase of $\varphi(r) = 0$. If the ground is highly conductive, a secondary magnetic field will be induced and superimposed on the primary field. This modifies the amplitude as well as the phase of the field $B_{\perp}(r)$. Therefore, increasing φ is an indicator of the conductivity of the ground and that of groundwater as well. This implicit information cannot be extracted yet from the SNMR data as it required coupled modeling of SNMR and electromagnetic induction, which is complicated.

The resolution and accuracy of the SNMR depend on $B_{\perp}(r)$ and decreases with depth. Higher currents $i_0$ and /or current durations τ are needed to excite the protons at greater depth (as long as $\tau << T_2^*$). By increasing q, the depth of the measurement is increased. In fact, the choice of q focuses the excitation to a certain depth range. Hence, measurements are conducted for different excitation intensities q. The main parameters for every q are the initial amplitude $E_o$ and the decay time T. The $E_o(q)$ and T(q) data sets are inverted, to find the distributions with depth of water content f(z) and of decay time T(z). The inversion is based on Eq. (3), which is used in a modified form for horizontal layering (Legchenko and Shushakov, 1998). Currently, various aspects of inversion are investigated and improvements envisaged (Yaramanci and Mohnke, 2000).

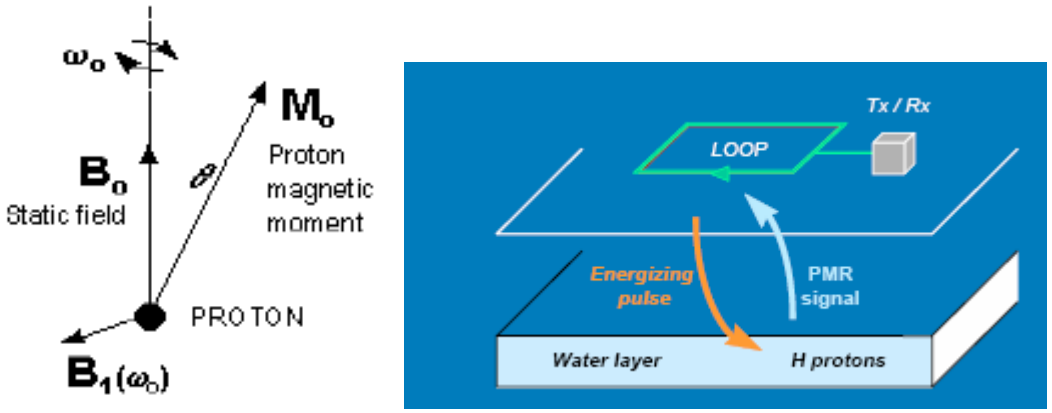


Energizing field

$$\omega_O = 2\Pi f_{Larmor} \qquad I_{(t)} = I_O \cos(\omega_{(L)} t)$$

Fig. 3.3: Basic of proton magnetic resonance sounding *(Iris instruments 1998)*

### *3.4.3 Data Acquisition*

The layout of the data acquisition is shown in Figure 3.2 and the procedure is outlined below. The geomagnetic field strength of the area is measured and an average is calculated to determine the Larmor frequency. This determined field is then put in the data acquisition system and a mini-sounding is then conducted for calibration purposes. The fine tuning adjustments are made in accordance with the response from the mini sounding.

A full sounding then follows. The stacking number (number of measurement to average-out a good stable signal value) depends on the noise level that is recorded before the start of each pulse.

Repeated measurements are made when corrupted values or anomalous values are obtained. Of note should be the monitoring of the geomagnetic strength during the survey, which may vary with time.

The MRS soundings were performed with the Numis system (Iris Instrument) using an antenna square shape loop 100 x 100 m. As the signal to noise ratio was high moderate stacking rates of 32 were quite sufficient. The frequencies have been around 1863Hz, corresponding to the total intensity of local Earth magnetic field of about 43 737 nT, very stable within $\pm 0.5Hz$ for all excitation intensities. The data were collected in three sites separated some 1400m.

### *3.4.4 MRS Inversion*

For the inversion of MRS data, the Samavor program provided with the commercial NUMIS system from IRIS Instrument was employed. The Tikhovov regularization method (Legchenko and Shushakvo 1998) has been used for model calculation (Legchenko and Villa 2002). The initial signal amplitude and the observed decay time as a function of pulse moment were used in the inversion to obtain a quantitative model of water content and the decay time $T_2^*$ distribution with depth. Two data files must be applied to the program for inversion; (1) a MRS recorded data file and (2) a designed matrix file. Parameters needed for the designed matrix file are: antenna type and size, number of wire turns used for the antenna, Larmor frequency, maximum depth of penetration defined in the matrix file, geomagnetic field inclination, maximum value of pulse moment, and a number of conductive layers.

The Larmor frequency is defined from the total local earth magnetic field, while the number of conductive layers can be estimated from e.g. interpretation of Vertical Electrical Soundings data. The maximum depth of penetration in the matrix file is defined from the antenna size (Samavor User's manual). The subsurface electrical conductivity at each measuring site is a major factor that influences to the depth of penetration (Shushakov 1996; Legchenko et al. 1997b).

The various physical hydro-geological parameters are reflected by: Amplitude of the NMR signal $E_o$ as a function of pulse moment q, which provides the water content, designated as $\Phi_{MRS}$ as a function of depth; Decay time constant $T_2^*$ as function of pulse moment q provides the pore size as a function of depth. The phase shift φ between signal and current as a function of pulse moment q is dependent on the rock layer conductivity.

### *3.4.5 Unsaturated Zone Parameter*

The water unsaturated zone in a soil is where chemical processes are at their most active. Its extent is determined by the content of water and cannot extend beyond the water table, below which voids are completely filled with water (Allavy, 1985.]. In this zone, there is gravitational water and capillary water including firmly bound water and loosely bound water see figure 3-4.

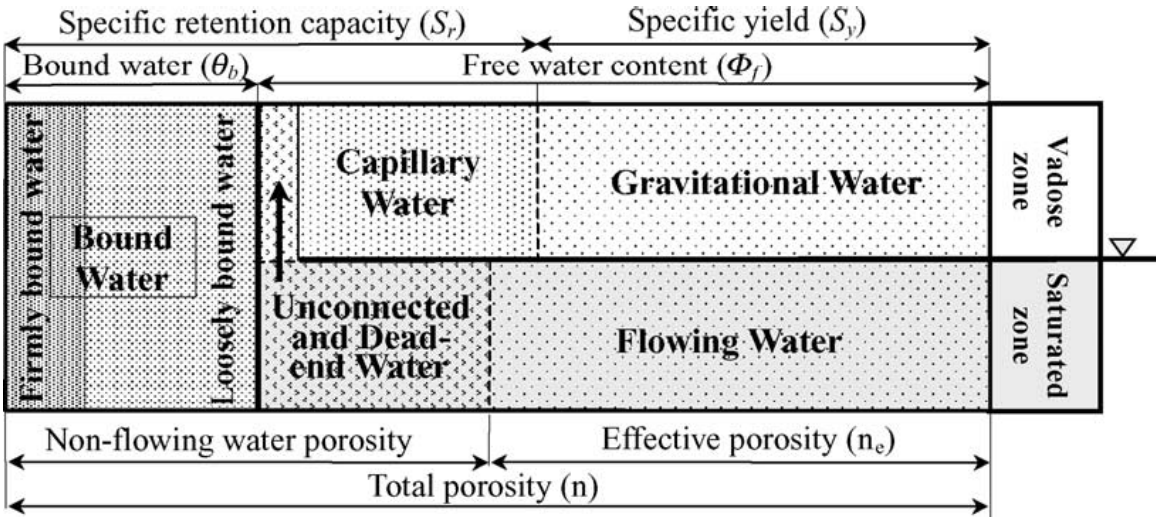


Figure 3-4: The Groundwater Storage Concept, after Lubczynski and Roy *(2003)*

### *3.5 Electrical Resistivity Survey*

The electrical resistivity in the subsurface varies between different geological materials, as shown in figure 3-5. Worth notice is that the resistivity of freshwater varies between approximately five to a hundred ohm-m due to different ion concentrations. Earth bulk material consists of a solid phase and a space phase. The most common minerals that form soils have very high resistivity in dry condition. The resistivity in the ground is therefore mainly depending on if the space phase is filled with water and if the water is rich in dissolved ions. Even if the porosity is rather low, the effect of water filled pores significantly reduces the resistivity. This means that electrical methods are useful for detecting groundwater tables if a distinct groundwater table exists. However, if the content of fine grained material is significant, the water content above the groundwater surface held by capillarity forces may be enough to dominate the electrical behaviour of the material.

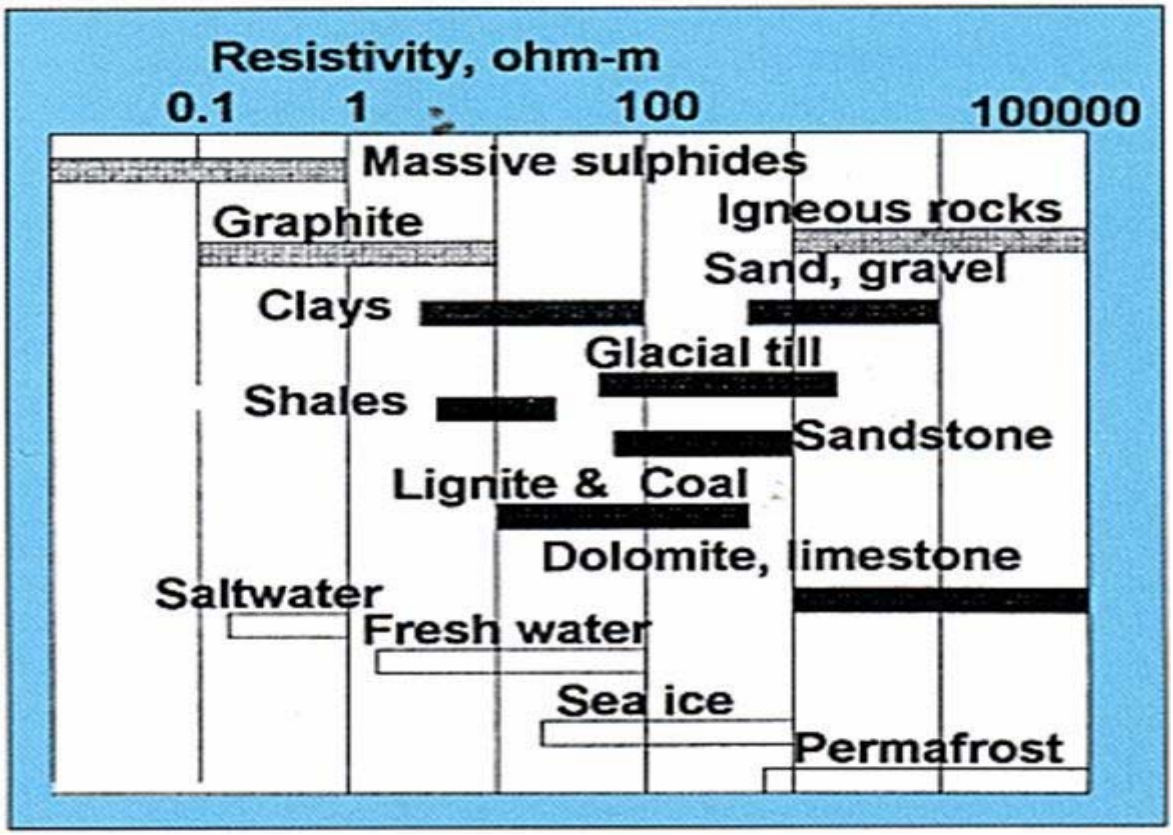


Figure 3-5. Typical ranges of electric resistivities of geological materials (Instruction manual ABEM)

In the most commonly used electrical methods, an electrical current is driven through the ground and the resulting potential differences are measured at the surface. Anomalous conditions or inhomogeneities within the ground, such as electrically better or poorer conducting layers, are inferred from the fact that they deflect the current and distort the normal potentials. This is the underlying principle of measuring subsurface variation in electrical resistivity (reciprocal of electrical conductivity) within the earth. The technique of resistivity surveying was developed by Conrad Schlumberger who conducted the first experiments (1912).

### *3.5.1 Resistivity Instruments*

Resistivity surveys can be carried out with simple equipment consisting of a high-voltage battery pack as the source of current (terrameter), four metal stakes, hammer, and four reels of insulated cable (Fig 3-6)

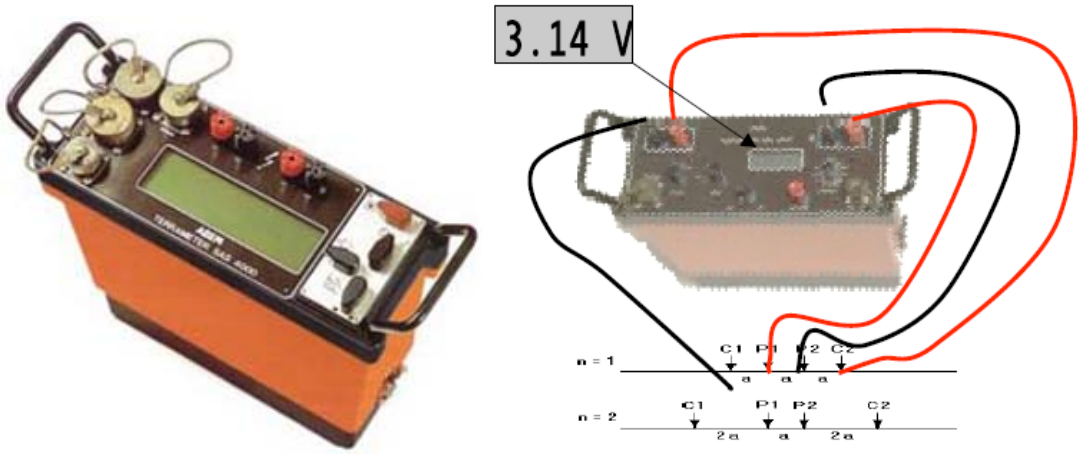


Fig. 3-6: Resistivity instrument and its layout

### *3.5.2 Electric Resistivity Investigation*

An electrical resistivity survey is based on the principle of rock material acting as a resistor in a circuit. The basic idea behind the electrical geophysical method is that different geologic materials have different electrical properties. An electrical current is induced into the ground. The ability of that material to resist the current is measured. Because different materials exhibit characteristic resistivity values, they can be distinguished by using this method. Factors that affect the resistivity are

porosity, pore-fluid content, temperature, and salinity. Soils are more conductive than rocks, and saturated clays are more conductive than dry sands. Changes in pore water salinity also have great impact on ground conductivity. Applications of the electrical resistivity method include locating aquifers, salt water intrusions, and other ground water contamination problems. They can characterize bedrock by locating weathered zones, fractures or determine depth to bedrock, and thickness of e.g. clay or sand layers.

Based on Sharma (1986), Telford (1990) and Milsom (1996) the property of the electrical resistivity of a material is usually expressed in terms of its resistivity. If the resistance between opposite faces of a conducting cylinder of length ℓ and cross-section areas **A** is ***R,*** the resistivity is expressed as

$$\rho = RA/\ell \qquad (6)$$

for an electrical circuit, Ohm's Law gives

$$R = \frac{V}{I} \qquad (7)$$

where V and I are the potential difference across a resistor and the current passing through it, respectively. The resistance (***R***) of the layer is specified by its length (ℓ) area of cross-section (**A**), and the resistivity (ρ). By definition equation 6 and equation 7 can be rewritten as

$$\frac{\Delta V}{\ell} = \frac{\rho I}{A} \qquad (8)$$

or

$$gradV = \frac{\rho}{I} \qquad (9)$$

The electrical current is directly introduced into the ground through current electrodes. The resulting voltage potential difference is measured between a pair of potential electrodes. The current and the potential electrodes are generally arranged in a linear pattern. The apparent resistivity is the bulk average resistivity of all soils and rock influencing the flow of current. The most often used electrode configurations are Wenner, Dipole-Dipole and Schlumberger configuration.

This study employed the simple Vertical Electrical Sounding (VES) in Schlumberger configuration. Equipment used was a fully automatic Terrameter (ABEM). In the generalized Schlumberger configuration, the spacing between potential electrodes is smaller than current electrodes. The current electrodes $\mathbf{C_1}$ and $\mathbf{C_2}$ are at equal distances **L** from the center of the array. The potential electrodes $\mathbf{P_1}$ and $\mathbf{P_2}$ are put between $\mathbf{C_1}$ and $\mathbf{C_2}$ at equal distances **b** from the center of the array. The current electrodes are located at a distance of **2L** from each other, and the potential electrode distance is **2b, 2L > 5MN** see figure 3.7. The survey uses an arrangement with a separation of 320 m and 10 m for location 5 and 6 respectively.

The measurement of apparent resistivity ($\rho_a$) is determined from Ohm's law using the potential difference (voltage) between two electrodes for a known current. At small distance between electrodes, the apparent resistivity is close to the resistivity of the upper layer. With distance between electrodes, more current passes through lower layers and the apparent resistivity changes. Apparent resistivity never reaches the resistivity of the lowest layers because some current always travels through the upper layers. Changes in apparent resistivity with electrode spacing depend on depth to the interface and the contrast in resistivity. At each electrodes separation, a value of apparent resistivity ($\rho_a$) is calculated using the measured resistance in conjugation with the appropriate **geometric factor** for the electrodes configuration. The values of apparent resistivity are plotted on a graph (field curve) the X- and Y- axes of which represent the logarithm values of the current electrodes half-separation (**L**) and the apparent resistivity ($\rho_a$), respectively.

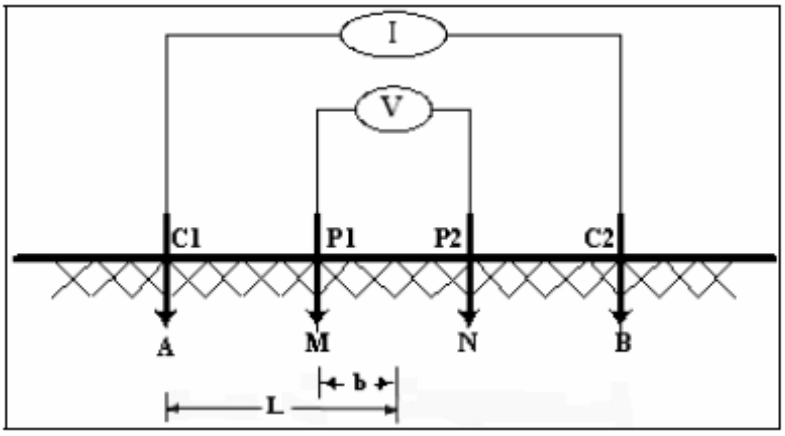


Figure 3.7 The Schlumberger configuration pattern.

In Figure 3.7, the source and sink electrodes are **A** and **B**, and the so-called potential electrodes are **M** and **N**. The **M** electrodes are at distances $\mathbf{C_1P_1}$ and $\mathbf{C_1P_2}$ from the source and sink, and the **N** electrodes are at distances of $\mathbf{C_2P_1}$ and $\mathbf{C_2P_2}$. According to Ohm's law, if the resistivity *R* is uniform, the electric potential $\mathbf{V_M}$ at the **M** electrodes will be

$$V_M = \frac{I\ell}{2\Pi}\left[\frac{1}{C_1P_1} - \frac{1}{C_1P_2}\right] \qquad (10)$$

and the potential $\mathbf{V_N}$ at the N electrodes will be

$$V_N = -\frac{I\ell}{2\Pi}\left[\frac{1}{C_2P_1} - \frac{1}{C_2P_2}\right] \qquad (11)$$

Therefore, the difference in potential $\mathbf{V_{MN}}$ measured by the voltmeter will be

$$\mathbf{V_{MN} = V_M - V_N} = \frac{I\ell}{2\Pi}\left[\frac{1}{C_1P_1} - \frac{1}{C_1P_2} - \frac{1}{C_2P_1} + \frac{1}{C_2P_2}\right] \qquad (12)$$

Equation (12) would then reflect average of resistivities in the difference materials within the zone between these equipotentials. Such a weighted average is called the apparent resistivity.

Defined as $\rho_a = \frac{V_{MN}K}{I}$ (13)

where **K** is geometrical factor which depends on the electrodes arrangement.

For the Schlumberger configuration, the geometrical factor is

$$\mathbf{K = \pi\,(L^2 - b^2)/2b} \qquad (14)$$

In this array, the depth to which the resistivity is averaged is roughly equal to half the separation between the current electrodes. Based on the equation (13) and (14), the apparent resistivity can be expressed by the formula:

$$\rho_a = \pi (L^2 - b^2) \qquad (15)$$

Where

L = the half-separation between the current electrodes (**A, B**) measured in meters;

b = the half separation between the measuring electrodes (**M, N**), in meters;

$\mathbf{V_{MN}}$ = the voltage at the measuring electrodes, in volts;

***I*** = the current between the current electrodes, in amperes.

This formula is based on the assumption that the ratio ***V/I*** is approximately equal to the voltage gradient, at the center of the electrode array.

The interpretation process consists of deducing a likely set of true resistivity values which would be compatible with the observed apparent resistivity values. In many cases, there exists no single set of resistivities that correspond to a particular set of apparent resistivities, and as such, the true resistivity cannot be uniquely determined. The apparent resistivity determined for a series of uniform horizontal layers, presents a geometrically simple case. Since this is frequently a good first approximation to geologic conditions, realistic model can be defined that involves determining layer thickness and resistivities that explain the measured apparent resistivities.

For conventional interpretation, the data are plotting on a graph paper i.e. the observed apparent resistivities against electrode distance. This is done in the same scale as for theoretical curves and the field data curve would be laid and moved over the theoretical curves until there is a match with the points of the theoretical curves. The depths and corresponding true resistivities are then read off of the field matched theoretical curve. However, this is time consuming and in exact. And an iterative matching program RESIST87 is here used for the interpretation.

### *3.6 Hydrochemical Techniques*

Water samples were collected at depth of 25 meter in boreholes located at points 9, 10 and 11 within the area (Fig.1-2). The water samples were carefully analyzed for the determination of chemical parameters. This was done at the Laboratory of Water Quality Analysis, Vientiane, Laos. A total of nine (9) parameters were determined but

the main interest was concentrated on Electrical Conductivity (EC), Chloride and Total Dissolved Solids (TDS).

### *3.7 Global Positioning System (GPS)*

The position of the sites for MRS data collection was determined by GPS. The GPS is developed by the US department of defence for determination of position. The navigation systems consist of 24 satellites, 5 ground stations for communication with the satellites and a GPS receiver for telling the satellites their position. The ground stations receive data from the satellites, correct them and then send the corrected data back to the satellites. Every satellite is continuously sending signals on two different frequencies. Civilian GPS use only one of the frequency, 1575, 47 MHz, in the UHF band. The signal can travel through clouds, glass and plastic, but will not travel thought solid object such as buildings and mountains. The GPS receiver has to know where the satellites are located and the distance to the satellites. The satellites are continuously sending out coded signals, which are telling the GPS the exact position of the satellites. The distance to the satellites is calculated from the simple formula, Velocity x Travel time = Distance, where the velocity is the same as that of light less any delay because the signal travel through the earth atmosphere. The travel time is estimated when a satellite generates a pseudo-random code and the GPS is generating the same code and tries to match it with the satellite code. The receiver then compares the two codes to determine how much it needs to delay its code to match the satellite code. The GPS clock does not keep the time as precise as the expensive satellite clock. For this reason, each distance measurement needs to be corrected to account for the GPS receiver's internal clock error. To correct this error, the GPS need to have contact with at least four satellites. It can be enough with three satellites during positioning, but the error will be greater. Here the positions are determined with an accuracy of $\pm 10 meters$.

Table 3-2: Location of MRS

| **MRS Location** | **Altitude** | **Northing** | **Easting** |
|---|---|---|---|
| 5 | 168 | 18.32905 | 102.65276 |
| 6 | 167 | 18.34009 | 102.64332 |
| 7 | 172 | 18.34072 | 102.65580 |

Table 3-3: Location of VES

| VES Location | Northing | Easting |
|---|---|---|
| 5 | 18.32904 | 102.6527 |
| 5-5 | 18.32787 | 102.6539 |
| 6 | 18.35022 | 102.6652 |

Table 3-4: Location of Well

| Well Location | Northing | Easting |
|---|---|---|
| 9 | 18.34006 | 102.6569 |
| 10 | 18.33047 | 102.6562 |
| 11 | 18.33774 | 102.6614 |

# 4.0 Presentation of Result and Discussion

## *4.1 1-D Interpretation*

Schlumberger array was used to acquire data for 1-D electrical surveys and the purpose of these soundings is to characterize the subsurface within the investigation

depth of the MRS soundings; hence a maximum AB/2 separation of 320 m was used, from which an investigation depth of at least ca 100 m could be expected. The centre of the schlumberger array was placed at the centre of MRS antenna loop.

Vertical electrical soundings (VES) were taken at location 5 and 6. The apparent resistivity values obtained from the field (Appendix I) were plotted on a log-log graph (Fig. 4.1) to obtain the sounding curves for the area. The vertical electrical sounding data were then interpreted using a computer iteration program known as RESIST version 1.0(Vander Velpen, 1988). The resistivity models were constrained by geological data from the drill-holes located in the vicinity of the measuring sites.

The sounding curves show geoelectrical layers of various resistivities and thicknesses as presented in table 4-1 and fig. 4.1.

Table 4-1: Summary of VES Result

| VES No | Geoelectrical Layer | Resistivity (Ωm) | Thickness (m) | Depth (m) |
|---|---|---|---|---|
| 5 | 1 | 489.4 | 2.6 | 2.6 |
| | 2 | 258.4 | 8.1 | 10.7 |
| | 3 | 32.5 | - | - |
| 6 | 1 | 965.8 | 1.1 | 1.1 |
| | 2 | 548.4 | 1.1 | 2.2 |
| | 3 | 59.3 | - | - |

It must be recalled that we encountered problem of layer inhomogeneity in the location 6. As we increased the current electrode separation, subsurface materials cause distortions in the current flow which give rise to corresponding irregularities in the values of potential difference. As a result, we were unable to probe farther than AB/2 of 10 meters.

A fit between the measured data and the calculated data is very good with RMS error <3 %. Three layers of different resistivity were detected both in the location 5 and 6.

The interpretation of the sounding curves can result in a number of models with reference to the equivalence rule between resistivity and layer thickness. Therefore the geological data from a borehole located close to the measuring locations are very important constraint for the modeling.

At location 5, the VES model shows three layers with resistivity of 489.4Ωm, 258.4Ωm, and 32.5Ωm respectively. The first layer is top soil of thickness 2.6 m, while the second layer is a sandy silt, with a of thickness 8.1 m. The third layer is composed of sand with clay and gravel. The thickness of this layer could not be determined as the current did not penetrate through the layer.

At location 6, the depth of penetration is very shallow. The first layer is the top soil of thickness 1.1 m and a resistivity of 965.8 Ωm. The second layer indicates a laterite with red silt of thickness 1.1 m and a resistivity of 548.4 Ωm. The third layer has a resistivity of 59.3 Ωm and probably is the first water aquifer in the area.

Location 5 (rms-error: 2.38)

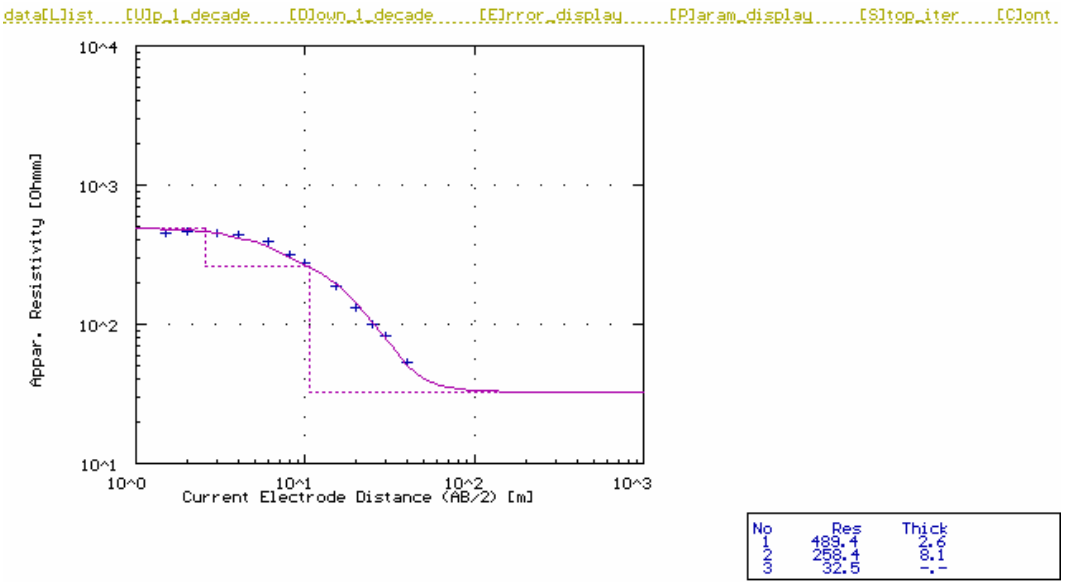


Location 6 (rms-error: 2.41)

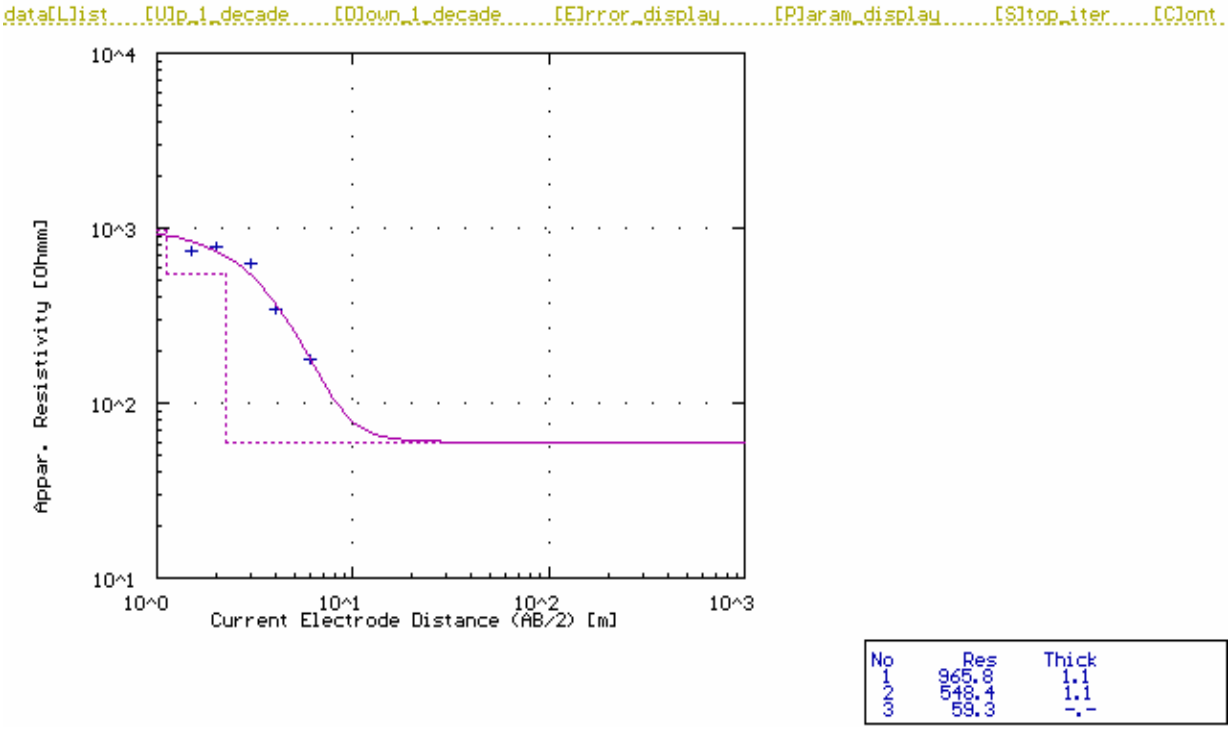


Figure 4-1 The VES interpretation shows the standard curve of the measured data fitting with the calculated data from the model of each measuring location

### *4.2 Magnetic Resonance sounding data*

The main parameters; $E_o$ (the initial maximum amplitude voltage or signal amplitude) and the observed decay time ($T_{2obs}^*$) indicate the content of subsurface water and mean pore size or porosity that is related to the permeability of the water storage materials respectively. Frequency and phase shift of the signal can be used for data quality control (Lubczynski and Roy 2003). According to Legchenko and Valla (2002) the MRS signal can be regarded produced by a proton magnetic resonance response if the phase and/or the frequency of the signal vary smoothly as the pulse moment increases.

The sounding curves of signal amplitude, the ambient noise levels, frequency and the phase shift from the location 5, 6 and 7 are plotted versus pulse moments in figure 4-2 e and f, figure 4-3 e and f, and figure 4-4 e and f respectively. A glance of hydrological characteristic at each location can be expressed by these curves before inverting the signal data of amplitude and $T_{2obs}^*$ as a function of pulse moments for a final model of water content and a decay time ($T_2^*$) with depth.

## Location 5

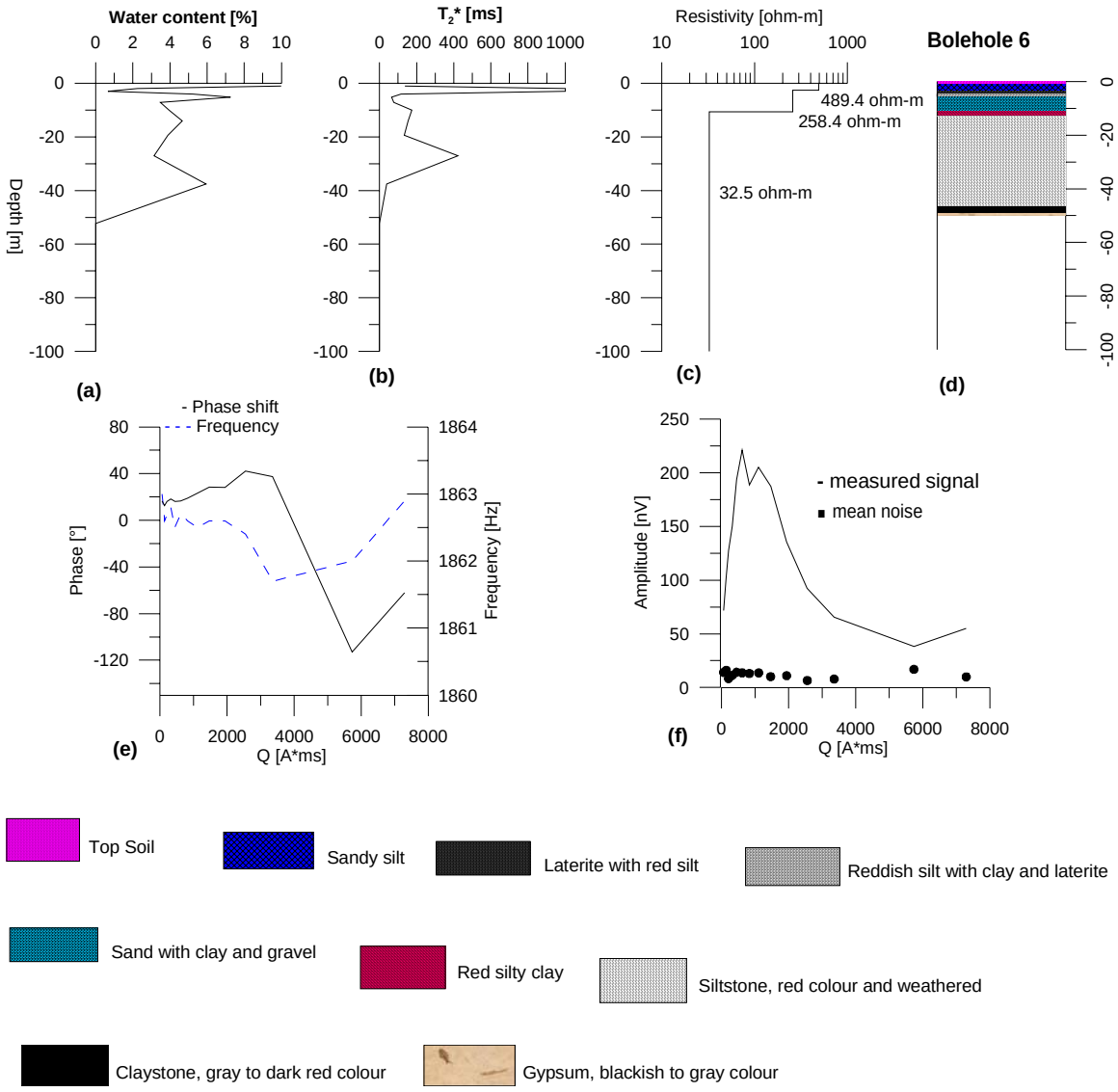


Fig 4-2: The MRS interpretations from the inversion model shows (a) the comparison between water content, (b) decay time, (c) SVES result, (d) the borehole data, (e) phase shift and frequency and, (f) measured signal and mean noise

## Location 6

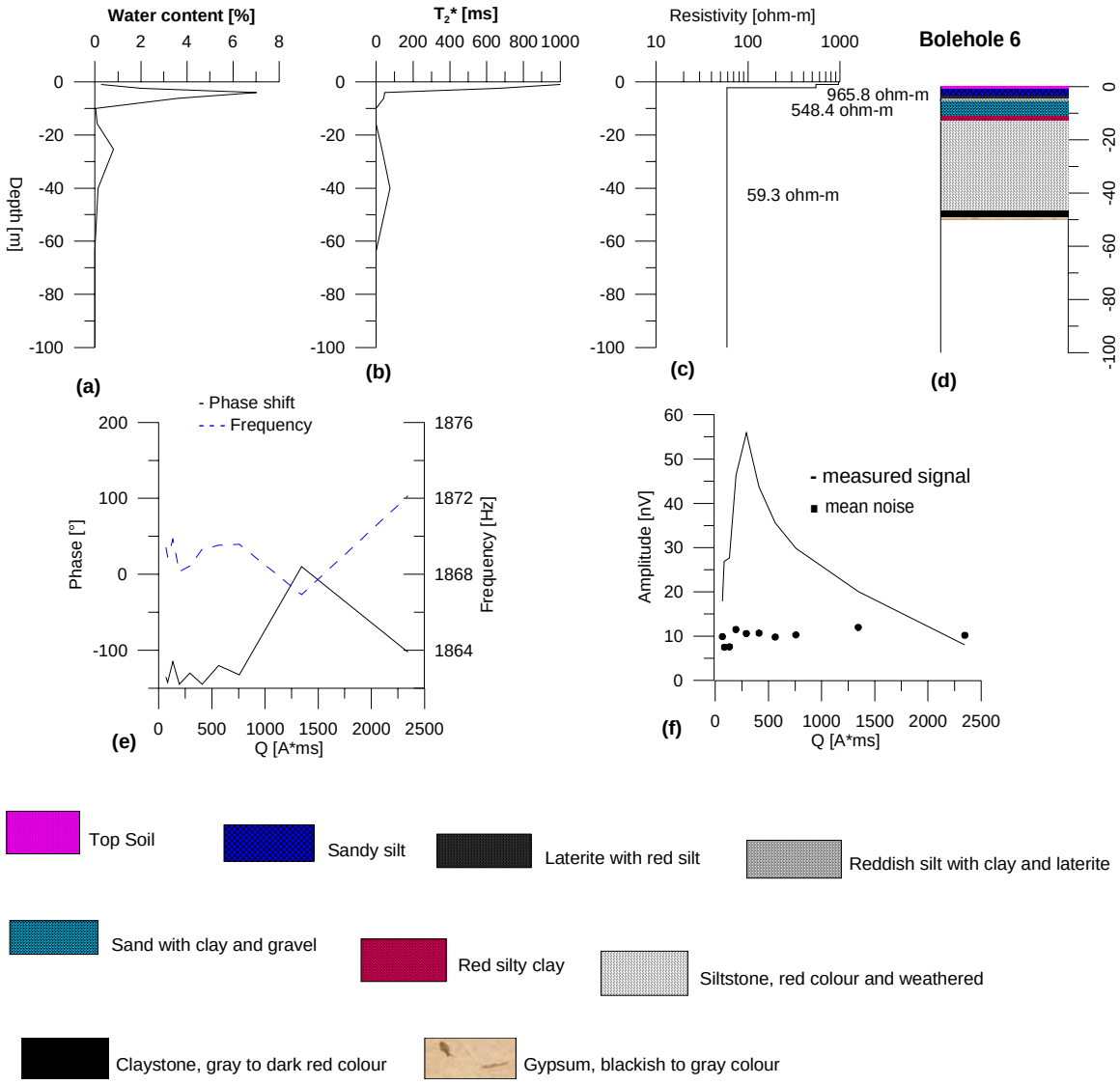


Fig 4-3: The MRS interpretations from the inversion model shows (a) the comparison between water content, (b) decay time, (c) SVES result, (d) the borehole data, (e) phase shift and frequency and, (f) measured signal and mean noise

## Location 7

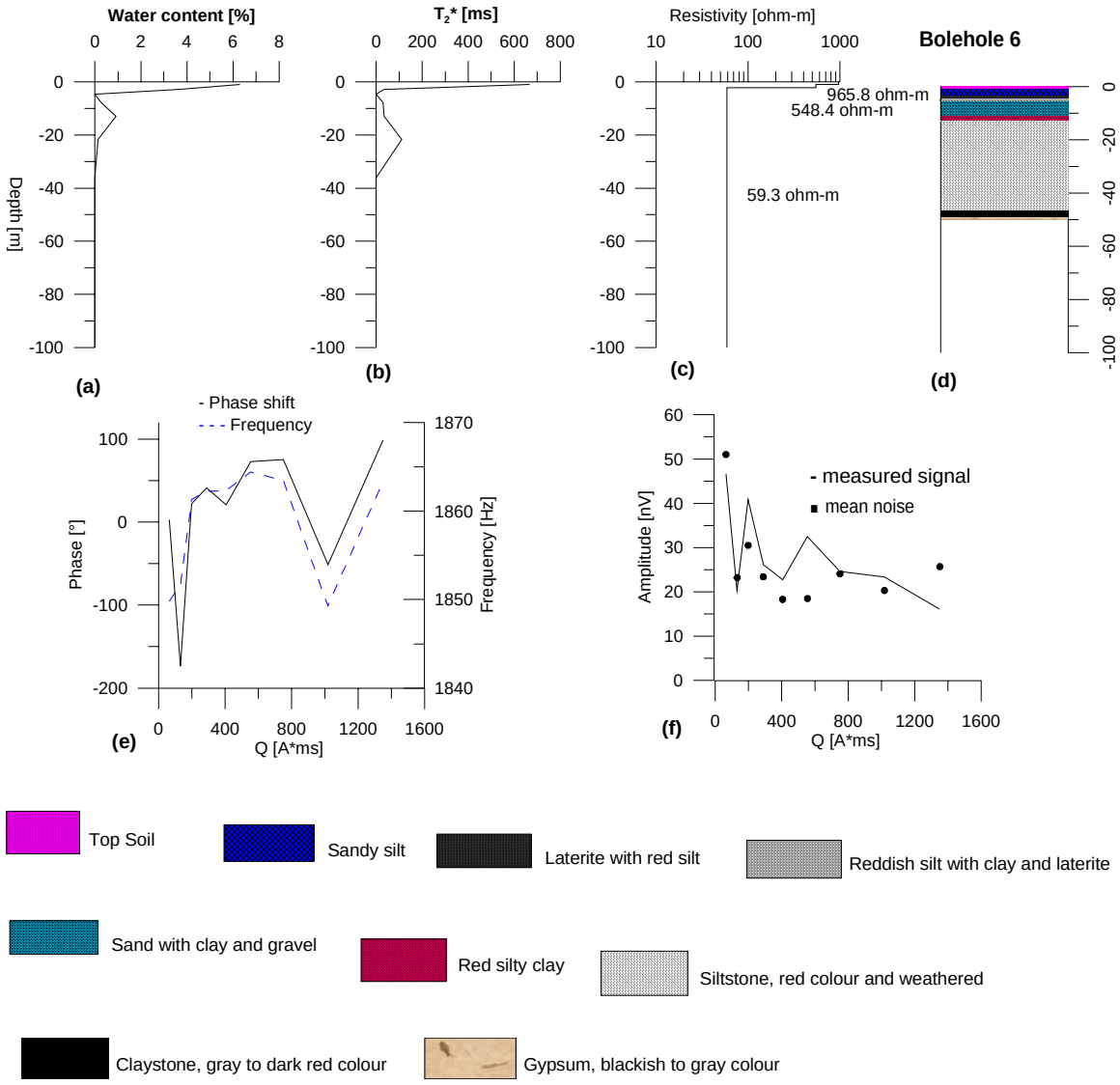


Fig 4-4: The MRS interpretations from the inversion model shows (a) the comparison between water content, (b) decay time, (c) SVES result, (d) the borehole data, (e) phase shift and frequency and, (f) measured signal and mean noise.

At MRS location 5 and 6 (fig. 4-2 e and f, and Fig.4-3 e and f) good quality data is expressed by the frequency. Only at location 7 (fig. 4-4 e and f), the frequency and the phase shift vary quite randomly with the pulse moments. This is consistent with high mean noise and low signal amplitude. The data from location 7 is thus less reliable.

The sounding curve at location 5 indicates only one aquiferous zone, which is reflected by the signal that starts at a pulse moment of 500 and runs to 4000 A-ms. The signal amplitude ranges from 170 to 225nV and the observed decay time varies between 100 to 420 ms. The curve gives information of structures close to the surface. With reference to an approximate correlation between observed relaxation time and type of geological strata (Schirov et al, 1991), this range of $T_{2obs}^{*}$ (200 – 400ms) may represent fine sand to medium sand, which corresponds well with the geological data from borehole 6.

At location 6, the sounding curve indicates one shallow water layer as reflected by the signal amplitude that starts at a pulse moment of 250 to 1500 A-ms. The signal amplitude ranges from 20 to 55 nV and $T_2^*$ varies between 60 to 100 ms. This decay time range represent fine sands.

The lowest signal amplitude is recorded at the location 7. In first part of the curve, at pulse moment is from 100 to 1300 A-ms, the signal amplitude ranges between 15 to 44 nV. This range of signal amplitude is within the mean noise level (fig. 4-3 f).
Thus there is no signal indicating any water bearing layer. Therefore, the upper part is probably an impermeable layer such as clay.

### *4.3 Result of the MRS Inversion*

From the MRS inversion, models of free water content and the decay time ($T_2^*$) distributions with depth (Legchenko and Valla, 2002) are obtained. The models can reflect major properties of an aquifer like aquifer geometry i.e. the hydrostratigraphic boundaries; unconfined groundwater table depth, layer boundaries, and aquifer parameters such as water content, storage parameters (storability and specific yield), flow parameters (hydraulic conductivity, permeability and transmissivity). For the position of the groundwater table, there is no universal and unique recipe to mark it by

using a combination of water content and the relaxation time. However, comparison with field hydrogeological data has shown that the groundwater table may be marked by inflection, bend or break point on either water content or on $T_2^*$ curve or on both of them(Lubczynski and Roy, 2003). For the evaluation of storage and flow, borehole pumping test data (hydrodynamic properties) is needed for calibration (Legchenko et al. 2002). In this project, there is no borehole pumping test data available that can be used for calibration.

At location 5, the best fit between the measured and the calculated signal was obtained when a maximum depth in the design matrix of 100 m was applied (fig 4-2f). The signal-to-noise ratio here is 6.59. The model indicates one water-bearing layer (fig. 4-2 a) for which the depth ranges from 2 m to 45 m and the water content ranges between 2 – 7.5 %. $T_2^*$ ranges roughly from 100 to 1000 ms, which corresponds to the sandy silt layer in borehole 6 located some few kilometers away from measured the site (fig 4-2 d).

At location 6 (fig 4-3), the best fit between the measured and the calculated data was achieved with a maximum depth of 100 m for the designed matrix (fig 4-3 f). Low initial maximum amplitude of the MRS signal and a S/N of 2.19 were observed. The model indicates one shallow water bearing formation running at depths from 0.5 m to 10 m, in which the water content ranges between 0.5 to 7.0 %. $T_2^*$ ranges roughly from 100 to 1000 ms and this may correspond to the sandy silt layer in borehole 6. There is a good agreement between the water content and $T_2^*$ (fig 4-3 a and b).

At location 7, the best fit between the measured and the calculated data was obtained with a maximum depth of 100 m for the designed matrix (fig. 4-4 f ). A very low initial maximum amplitude of the MRS signal (< 50 nV) and a S/N of 1 were observed. At shallow depth, where the pulse moment was < 400 A-ms, the signal amplitude was within the noise level. This means that there was no water indicated at this depth or that the signal was attenuated by a high conductive layer.

### *4.4 Hydrochemical Analysis*

Hydrochemical analysis results of water samples taken at a depth of 25 meters in boreholes located at points 9, 10 and 11 within the area (Fig.1-2) are presented in table 4-2. The water samples were carefully analyzed for the determination of chemical parameters. This was done at the Laboratory of Water Quality Analysis,

Vientiane, Laos. A total of nine (9) parameters were determined but here I concentrated on Electrical Conductivity (EC), Chloride and Total Dissolved Solids (TDS) content.

Table 4-2 Water Quality Analysis Report

| Item | Parameter | Unit | Borehole 9 | Borehole 10 | Borehole 11 |
|---|---|---|---|---|---|
| 1 | EC | μS/m | 9.20 | 27.70 | 47.00 |
| 2 | TDS | mg/l | 46.00 | 139.00 | 15.00 |
| 3 | Ca | mg/l | 9.70 | 24.60 | 2.40 |
| 4 | Mg | mg/l | 2.80 | 9.10 | 0.70 |
| 5 | Na | mg/l | 4.70 | 16.90 | 2.70 |
| 6 | K | mg/l | 0.50 | 2.20 | 0.20 |
| 7 | Alkalinity | mg/l | 14.90 | 42.80 | 2.40 |
| 8 | S04 | mg/l | 5.50 | 26.50 | 1.30 |
| 9 | Cl | mg/l | 18.10 | 47.20 | 7.90 |

### *4.4.1 Total Dissolved Solids (TDS)*

Total Dissolved Solids refer to any minerals, salt, metals, cations or anions dissolved in water. In general, the TDS concentration is the sum of the cations and anions in the water. TDS comes from organic sources and inorganic minerals. World Health Organization (WHO) and United State Environmental Protection Agency (USEPA) advise a maximum contamination level of 500mg/l for TDS. Numerous water supplies exceed this level in some areas. When TDS levels exceed 1000mg/l, it is generally considered unfit for human consumption. The ranges of TDS and the limit for human consumption are shown in figure 4-5. For these water samples, the values of TDS are 46, 139 and 15 mg/l for borehole 9, 10 and 11, respectively, which are not up to the contaminated level. The comparison of TDS values against each well is shown in fig. 4.6

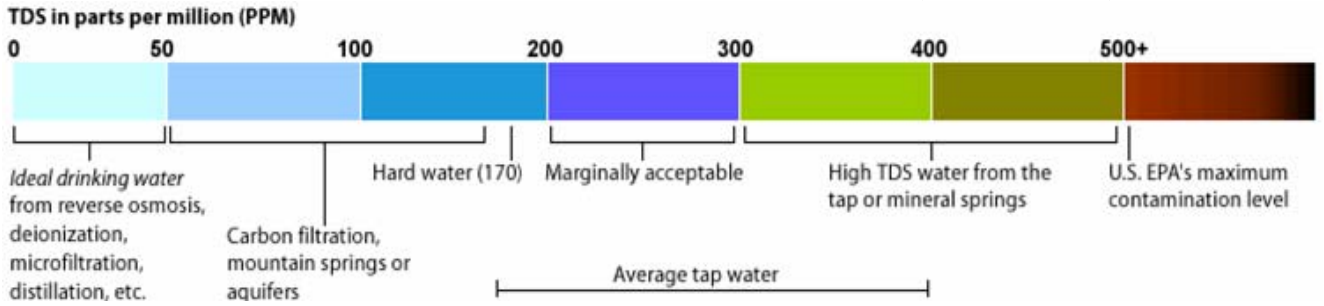


Fig.4.5: The ranges of TDS and the fitness of water for human consumption (http://www.tdsmeter.com/abouttds.html)

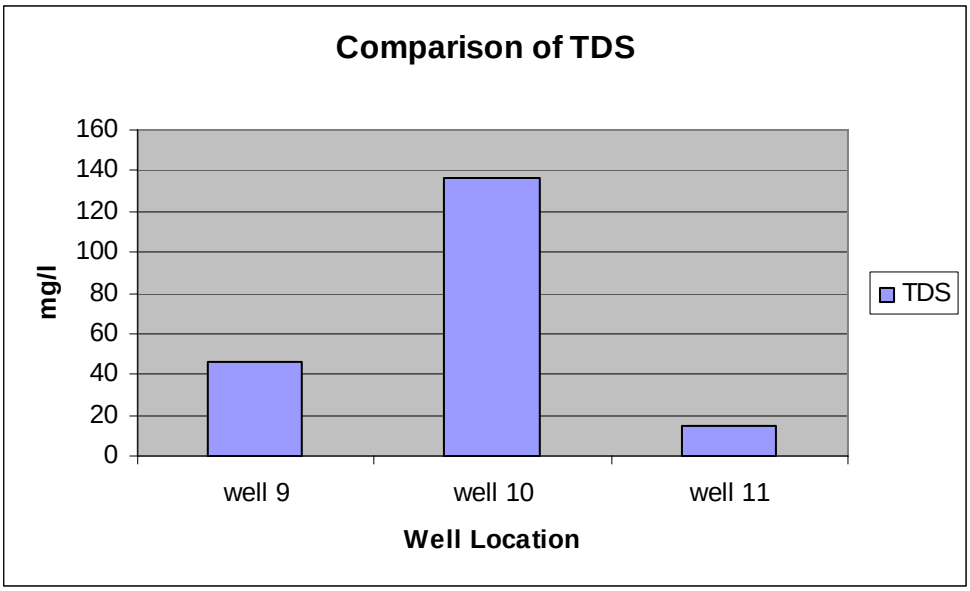


Fig. 4.6: The comparison of TDS values against well location

### *4.4.2 Chloride*

Chloride is a chemical commonly found in soil and rocks. It belongs to the halogen group and is very mobile in groundwater. The primary source of chloride is halite (salt) and brines. Anthropogenic (human) sources of chloride include fertilizer, road salt, human and animal waste and industrial applications. These sources can result in significant concentration of chloride in shallow groundwater because chloride is readily transported through the soil. High concentration of chloride gives a salty taste to water and the maximum concentration for drinking water is, according to World Health Organization 250mg/l. For the water samples of this study, the values of

chloride are 18.1, 47.2 and 7.9 mg/l for borehole 9, 10 and 11, respectively, which are not up to the contaminated level.

The comparison of chloride values against each well is shown in fig. 4.7.

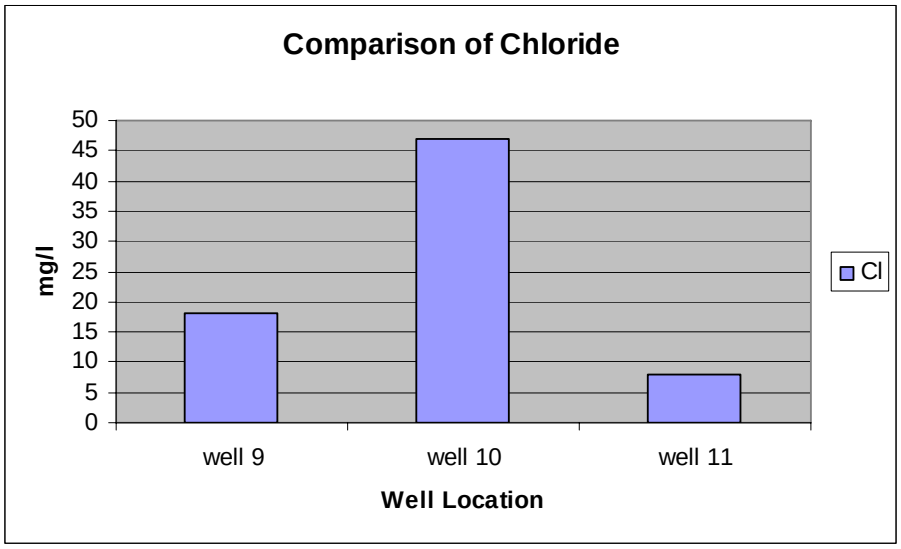


Fig. 4.7: Comparison of Chloride values against the well location

### *4.4.3 Electrical Conductivity*

Electrical conductivity is a measure of the ability to conduct an electrical current through a given solution and is used to indicate the total salt content or Total Dissolved solids, for a given water at a specific site. The more salts in the water, the better conductor it becomes. The strength of the electrical current is dependent upon the temperature of the solution and type of concentration of ion within the solution. Since the EC of water is strongly related to the salt concentration, the European Union (EU) directive on water quality (1998) sets an upper limit of 2500µs/cm for the electrical conductivity of drinking water. For the water samples of this study, the values of EC are 9.2, 27.7 and 47.0 uS/m for borehole 9, 10 and 11, respectively, which are not up to the contaminated level. The comparison of chloride values against each well is shown in fig. 4.8

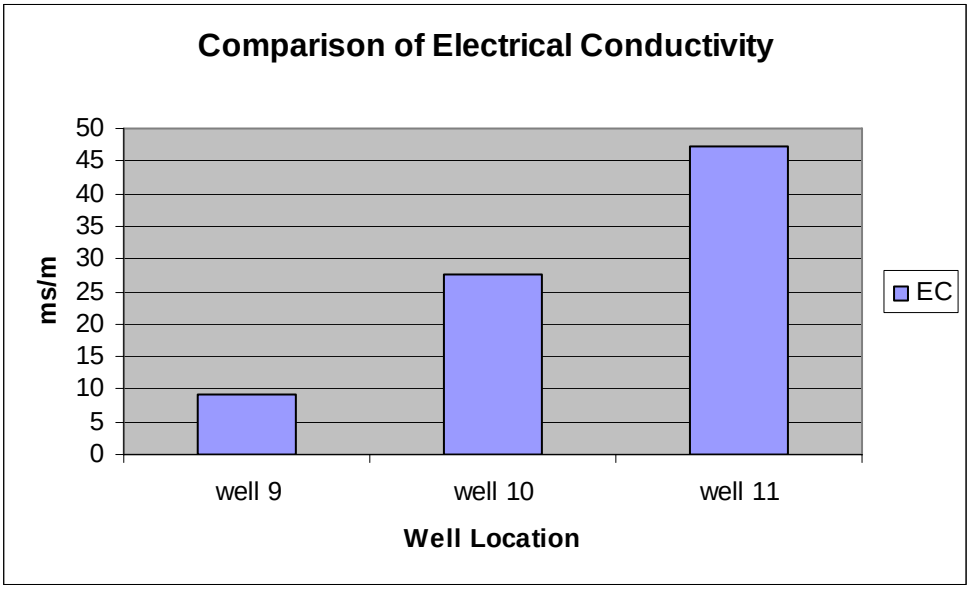


Fig. 4.8: Comparison of Electrical conductivity values against the well location

## 5.0 Summary and Conclusion

The Magnetic Resonance Soundings has been proven to be an efficient tool in groundwater exploration in the area of high magnitude of earth magnetic field, in Laos. Good quality data were obtained since measuring position is less affected by ambient noises, the variation of earth magnetic field and the magnetic susceptibility of subsurface or surface soil. The frequency and phase shift variation with pulse moments are not used in a standard inversion tool but they benefit in data acquisition quality control and interpretation results.

The inversion of Magnetic Resonance data $E_o$ (Q) and T(Q) provided reliable information on depth, thickness D, water content ($\phi$) for each of the water carrying layers of the study area. The correlation between the water content and the decay time reflect to the properties of water storage materials. The MRS results obtained in the location 6 agreed well with the result of VES as water-bearing formation is at shallow depth which also agrees well with the geological data provided by borehole 6.
The low signal amplitude at location 7 might be caused by attenuation due to a highly conductive layer overlay on the top of the aquifer or due to absence of water.
The highest water content (2.0- 7.5 %) was delineated at location 5 in depths between 2 and 45 m. This agreed with results obtained both in the VES and borehole data.

Schlumberger VES has successfully detected subsurface geological variation in the study area, however geological data are needed for constraining the interpretation.
Unfortunately, VES could not give the information of deeper parts as the AB/2 terminated at 320 m. However good results were obtained from shallow depths, results that are generally consistent with the MRS results. The reason for the limited depth penetration is probably due to high conductive layers and/or inhomogeneity of subsurface.
The MRS and VES data would give more reliable 2-dimensional images of the hydrogeology if there was more information from more sites. More details of the geology could also be obtained if other geophysical methods such as Ground Penetrating Radar, Refraction seismic and Electromagnetic methods were applied.

The hydrochemical analysis of the water samples show that the water is fit for drinking without causing health risk, with reference to standard established by the World Health Organization (WHO) and United State Environmental Protection Agency (USEPA).

The result of the study shows that the most favorable spots to drill for a deeper aquifer can be found in the area of location 5 where water can be found to depth of 40 m. Shallow aquifer with a maximum depth of 20 m can be drilled at location 6. We could not define any aquifer in location 7.

## 6.0 References

Achache, J., Courtillot, V., Besse, J., 1983. Paleomagnetic constraints on the late Cretaceous and Cenozoic tectonics of southeastern Asia. Earth Planet. Sci. Lett. 63, 123–136.

Cooper, M.A., Herbert, R., Hill, G.S., 1989. The structural evolution of Triassic intermontane basins in northeastern Thailand. In: Thansuthipitak, T. (Ed.), Proceedings International Symposium on Intermontane Basins: Geology and Resources, Chiang Mai, pp. 231-242

Dingman, 1994. S.L. Dingman. *Physical Hydrology*, Macmilan Publishing Company (1994).

Drumm, A., Heggemann, H., Helmcke, D., 1993. Contribution to the sedimentology and sedimentary petrology of the non-marine Mesozoic sediments in northern Thailand (Phrae and Nan Provinces). Int. Symp. Biostratigraphy of Mainland Southeast Asia: Facies and Paleontology, 31 January–5 February, Chiang Mai, pp. 299–318.

Dunn et al., 1999. K.J. Dunn, G.A. La Torraca and D.J. Bergman, Permeability relation with other petrophysical parameters for periodic porous media. *Geophysics* **64** 2 (1999), pp. 470–478.

Elming and Wattanasen, 2007. Direct and indirect methods for groundwater investigation; case-study of MRS and VES in the southern part of Sweden

Fetter, 1994. C.W. Fetter. *Applied Hydrogeology*, Prentice Hall, New Jersey (1994)

Gardner, L.S., Haworth, H.F., Na Chiengmai, P., 1967. Salt resources of Thailand. Rep. Invest. DMR, Bangkok, 100 pp.

Gev et al., 1996. I. Gev, M. Goldman, B. Rabinovich, M. Rabinovich and A. Issar, Detection of the water level in fractured phreatic aquifers using nuclear magnetic resonance (NMR) geophysical measurements. *Journal of Applied Geophysics* **34** (1996), pp. 277–282.

Goldman et al., 1994. M. Goldman, B. Rabinovich, M. Rabinovich, D. Gilad, I. Gev and M. Schirov, Application of the integrated NMR-TDEM method in groundwater exploration in Israel. *Journal of Applied Geophysics* **31** (1994), pp. 27–52.

Greiner et al., 1997. A. Greiner, W. Schreiber, G. Brix and W. Kinzelbach, Magnetic resonance imaging of paramagnetic tracers in porous media: quantification of flow and transport parameters. *Water Resources Research* **33** 6 (1997), pp. 1461–1473.

Hertrich and Yaramanci, 2002. M. Hertrich and U. Yaramanci, Joint inversion of surface nuclear magnetic resonance and vertical electric soundings. *Journal of Applied Geophysics* **50** (2002), pp. 179–191.

IRIS Instruments, 2002. IRIS Instruments, 2002. www.iris-instruments.fr/.

Institute for Global Environmental Strategies, IGES 1987

Japan International Cooperation Agency, Lao People's Democratic Republic, Ministry of Public Health, 1992

Kenyon et al., 1989. Kenyon, W.E., Howard, J.J., Sezginer, A., Straley, C., Matteson, A., Horkowitz, K., Ehrlich, R., 1989. Pore-size distribution and NMRin microporous cherty sandstones. SPWLA 13th Annual Logging Symposium, Paper LL.

Kgotlhang, 2000. Evaluation of the magnetic resonance sounding technique as a tool for groundwater exploration. Case study—Botswana. Msc thesis. Library of ITC.

Legchenko et al., 1995. A.V. Legchenko, O.A. Shushakov, J.A. Perrin and A.A. Portselan, Noninvasive NMR study of subsurface aquifers in France. *Annual Meeting SEG Houston* (1995).

Legchenko et al., 1998. Legchenko, A.V., Baltassat, J.M., Beauce, A., Makki, M.A., Al-Gaydi, B.A., 1998. Application of the surface proton magnetic resonance method for the detection of fractured granite aquifers. Proceedings of the IV Meeting of the Environmental and Engineering Geophysical Society, September 14–17, 1998, Barcelona, pp. 163–166.

Legchenko et al., 2002. A. Legchenko, J.M. Baltassat, A. Beauce and J. Bernard, Nuclear magnetic resonance as a geophysical tool for hydrogeologists. *Journal of Applied Geophysics* **50** (2002), pp. 21–46.

Lubczynski, 1997. Lubczynski, M.W., 1997. Application of numerical flow modelling combined with remote sensing and GIS techniques for the quantification of regional groundwater resources in hard rock terrains. IAHS Publication No. 241.

Lubczynski and Roy, 2004. M.W. Lubczynski and J. Roy, Magnetic resonance sounding (MRS) – new method for groundwater assessment. *Ground Water* 42 (2004).

Marsily, 1986. G. Marsily. *Quantitative Hydrogeology*, Academic Press, New York (1986).

Ministry of Agriculture and forestry, Laos PDR, 1998

Mohnke et al., 2001. Mohnke, O., Braun, M., Yaramanci, U., 2001. Inversion of decay time spectra from surface-NMR data. Proceedings of Seventh Meeting of Environmental and Engineering Geophysics, Birmingham, Great Britain.

Oswald et al., 1997. S. Oswald, W. Kinzelbach, A. Greiner and G. Brix, Observation of flow and transport processes in artificial porous media via magnetic resonance imaging in three dimensions. *Geoderma* 80 (1997), pp. 417–429.

Racey, A., Goodall, J.G.S., Love, M.A., Polachan, S., Jones, P.D., 1994. New age data for the Mesozoic Khorat group of northeast Thailand. Proc. Int. Symp. Stratigraphic Correlation of Southeast Asia, Bangkok, pp. 245–252.

Reinken et al., 1995. G. Reinken, F. Fuehr, N. Zadgorsky, H. Halling and O. Schult. *BCPC Monogr* **62** (1995), pp. 39–44.

Roy et al., 1998. Roy, J., Costa, A.M., Lubczynski, M.W., Owuor, C., 1998. Tests of the SGW-NMR technique within two aquifer characterization projects in the Iberian Penisula. Proceedings of the IV EEGS-ES Meeting, September14–17 1998, Barcelona, pp. 177–180.

Roy, 2000. Roy, J., 2000. MRS surveys under favorable conditions of S/N ratio. Proceedings of the Sixth Meeting of EEGS-ES, September 3–7, 2000, Bochum, Germany, P-EM-08.

Roy and Lubczynski, 2000a. Roy, J., Lubczynski, M.W., 2000a. MRS: introduction to a new geophysical technique and its current status; 1ero Congreso Cubano de Geofisica, Memorias de Geoinfo (Proceedings on CD-ROM).

Roy and Lubczynski, 2003. J. Roy and M.W. Lubczynski, The MRS technique and its use for groundwater investigations. *Hydrogeology Journal* **11** 4 (2003), pp. 455–465.

Sattayarak, N., Polachan, S., Charusirisawad, R., 1991. Cretaceous rock salt in the northeastern part of Thailand. Proc. 7th Reg. Conf. Geology and Mineral Resources Southeast Asia (GEOSEA VII), Bangkok.

Schirov et al., 1991. M. Schirov, A. Legchenko and G. Creer, A new direct non-invasive groundwater detection technology for Australia. *Exploration Geophysics* **22** (1991), pp. 333–338.

Sen, Zekai (1995); Applied Hydrogeology for scientist and Engineers. ISBN:1-56670-091-4

Sengor, C.A.M., 1979. Mid-Mesozoic closure of Permo-Triassic Tethys and its implications. Nature 279, 590–593.

Sengor, A.M.C., 1984. The Cimmeride orogenic system and the tectonics of Eurasia. Geol. Soc. Am. Spec. Pap. 195, 82 pp.

Semenov, 1987. A.G. Semenov, NMR HYDROSCOPE for water prospecting. *Proceedings of the seminar on Geotomography, Indian Geophysical Union, Hyderabad* (1987), pp. 66–67.

Sen et al., 1990. P.N. Sen, C. Straley, W.E. Kenyon and M.S. Whittingham, Surface-to-volume ratio, charge density, nuclear magnetic relaxation and permeability in clay bearing sandstones. *Geophysics* **55** 1 (1990), pp. 61–69.

Smith, P.F.L., Stokes, R.B., Bristow, C., Carter, A., 1996. Mid-Cretaceous inversion in the northern Khorat Plateau of Laos PDR and Thailand. In: Hall, R., Blundell, D.J.

(Eds.), Tectonic Evolution of Southeast Asia. Geol. Soc. London Spec. Publ. 106, 233–246.

Timur, 1969. A. Timur, Pulsed nuclear magnetic resonance studies of porosity, moveable fluid and permeability of sandstone. *Journal of Petroleum Technology* **21** 6 (1969), pp. 775–786.

Todd, 1959. K.D. Todd. *Groundwater Hydrology*, Wiley, New York (1959).

WCS (Wellfield Consulting Services), 1994. WCS (Wellfield Consulting Services). *Palla Road Groundwater Resources Investigation*, Ministry of Water Affairs of Botswana (1994).

WHO, (1988) International standards for drinking water. World Health Organization, Geneva

Yaramanci et al., 1999. U. Yaramanci, G. Lange and K. Knödel, Surface NMR within a geophysical study of an aquifer at Haldensleben (Germany). *Geophysical Prospecting* **47** (1999), pp. 923–943.

Yaramanci et al., 2002. U. Yaramanci, G. Lange and M. Hertrich, Aquifer characterization using Surface NMR jointly with other geophysical techniques at the Nauen/Berlin test site. *Journal of Applied Geophysics* **50** (2002), pp. 47–65.

# Appendix I

| **VES Schlumberger Configuration** | | | **Location 6** | | |
|---|---|---|---|---|---|
| | | | | | |
| **Observation No** | **MN/2 (m)** | **AB/2 (m)** | **R (Ohm)** | **K** | **Apparent .Resistivity = K*R** |
| 1 | 0.5 | 1.5 | 115.54 | 6.3 | 725.5912 |
| 2 | 0.5 | 2 | 64.859 | 11.8 | 765.3362 |
| 3 | 0.5 | 3 | 22.339 | 27.5 | 614.3225 |
| 4 | 0.5 | 4 | 6.669 | 49.4 | 329.4486 |
| 5 | 1 | 4 | 14.482 | 23.5 | 340.327 |
| 6 | 1 | 6 | 3.246 | 54.9 | 178.2054 |
| 7 | 1 | 8 | 0.037906 | 99.0 | 3.752694 |
| 8 | 1 | 10 | 0.024971 | 155.0 | 3.870505 |
| 9 | 2 | 10 | | 75.0 | 0 |
| 10 | 2 | 15 | | 173.0 | 0 |
| 11 | 2 | 20 | | 310.0 | 0 |
| 12 | 5 | 20 | | 118.5 | 0 |
| 13 | 5 | 25 | | 188.5 | 0 |
| 14 | 5 | 30 | | 274.8 | 0 |
| 15 | 5 | 40 | | 494.5 | 0 |
| 16 | 5 | 50 | | 777.0 | 0 |
| 17 | 10 | 50 | | 376.0 | 0 |
| 18 | 10 | 60 | | 549.5 | 0 |
| 19 | 10 | 80 | | 989.1 | 0 |
| 20 | 10 | 100 | | 1554.3 | 0 |
| 21 | 20 | 100 | | 753.6 | 0 |
| 22 | 20 | 120 | | 1099.0 | 0 |
| 23 | 20 | 140 | | 1502.0 | 0 |
| 24 | 20 | 160 | | 1978.0 | 0 |
| 25 | 20 | 180 | | 2512.0 | 0 |
| 26 | 20 | 200 | | 3100.0 | 0 |
| 27 | 40 | 200 | | 1507.0 | 0 |

| **VES Schlumberger Configuration** | | | **Location 5** | | |
|---|---|---|---|---|---|
| **Observation No.** | **MN/2 (m)** | **AB/2 (m)** | **R (Ohm)** | **K** | **Apparent Resistivity = K*R** |
| 1 | 0.5 | 1.5 | 72.081 | 6.3 | 452.66868 |
| 2 | 0.5 | 2 | 38.859 | 11.8 | 458.5362 |
| 3 | 0.5 | 3 | 16.378 | 27.5 | 450.395 |
| 4 | 0.5 | 4 | 8.9004 | 49.4 | 439.67976 |
| 5 | 1 | 4 | 23.376 | 23.5 | 549.336 |
| 6 | 1 | 6 | 8.991 | 54.9 | 493.6059 |
| 7 | 1 | 8 | 4.0247 | 99.0 | 398.4453 |
| 8 | 1 | 10 | 2.245 | 155.0 | 347.975 |
| 9 | 2 | 10 | 4.7138 | 75.0 | 353.535 |
| 10 | 2 | 15 | 1.3697 | 173.0 | 236.9581 |
| 11 | 2 | 20 | 0.53574 | 310.0 | 166.0794 |
| 12 | 5 | 20 | 1.4614 | 118.5 | 173.1759 |
| 13 | 5 | 25 | 0.7073 | 188.5 | 133.32605 |
| 14 | 5 | 30 | 0.39488 | 274.8 | 108.513024 |
| 15 | 5 | 40 | 0.14059 | 494.5 | 69.521755 |
| 16 | 5 | 50 | 0.0014533 | 777.0 | 1.1292141 |
| 17 | 10 | 50 | 0.0028414 | 376.0 | 1.0683664 |
| 18 | 10 | 60 | 0.0011326 | 549.5 | 0.6223637 |
| 19 | 10 | 80 | 0.0002756 | 989.1 | 0.27259596 |
| 20 | 10 | 100 | 0.0001353 | 1554.3 | 0.21029679 |
| 21 | 20 | 100 | 0.0003608 | 753.6 | 0.27189888 |
| 22 | 20 | 120 | 0.0006916 | 1099.0 | 0.7600684 |
| 23 | 20 | 140 | 0.0002255 | 1502.0 | 0.338701 |
| 24 | 20 | 160 | 0.000446 | 1978.0 | 0.882188 |
| 25 | 20 | 180 | | 2512.0 | 0 |